AD-A034 173 UTAH UNIV SALT LAKE CITY MICROWAVE DEVICE AND PHYSI--ETC F/G 17/8
SOLID STATE OPTICAL DETECTOR.(U)
AUG 76 R W GROW, J R BOYE, C K PETERSON N00014-67-A-0325-0005
UNCLASSIFIED UTEC-MD-76-233 NL

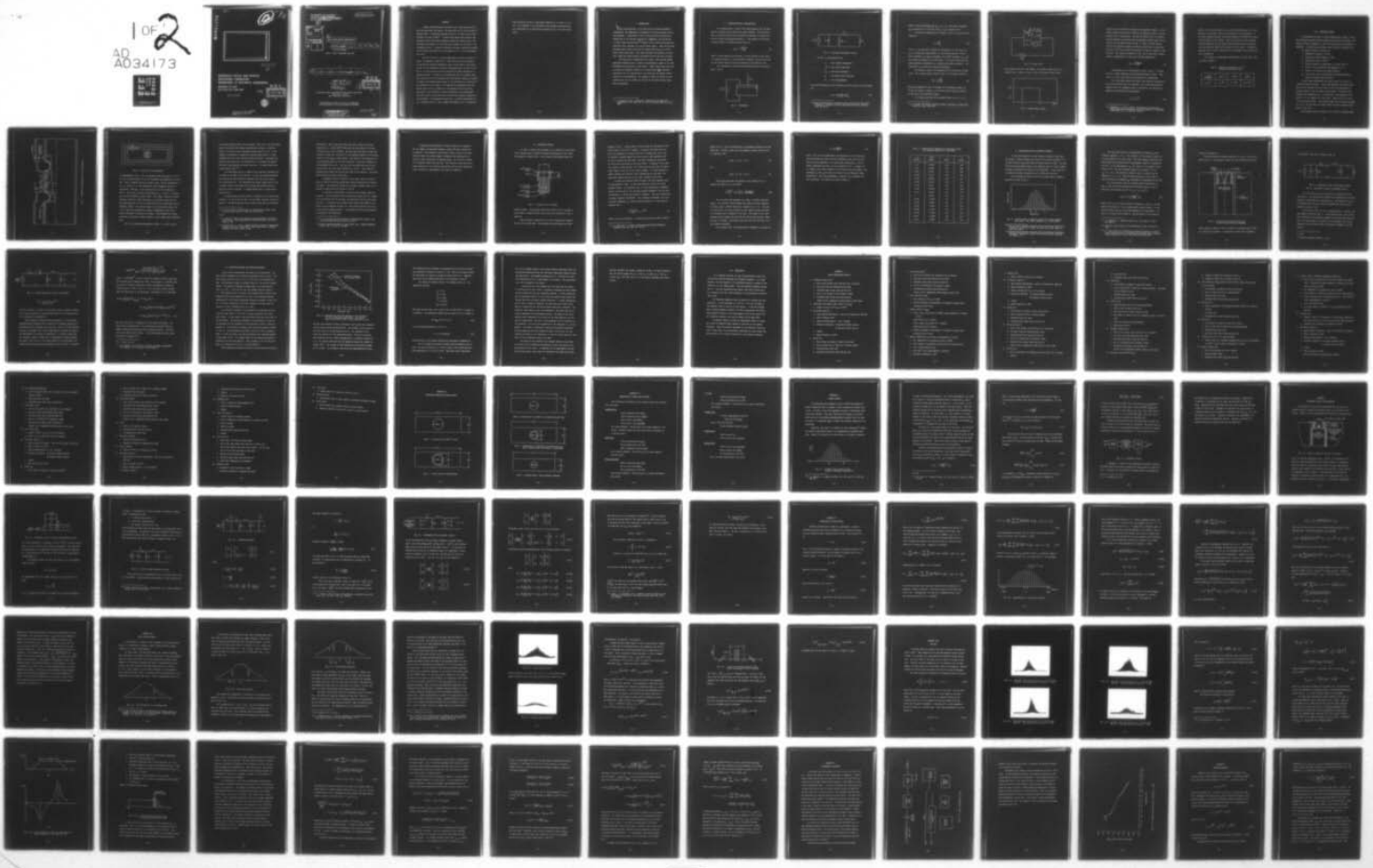

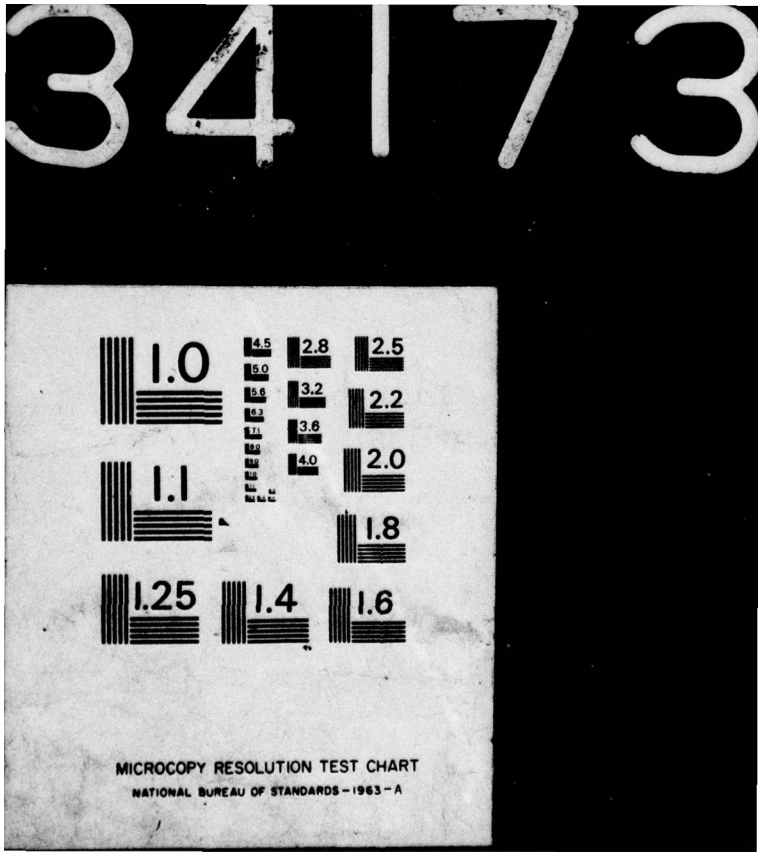
34173
1.0
1.1
1.25
1.4
1.6
1.8
2.0
2.2
2.5
2.8
3.2
3.6
4.0
4.5
5.0
5.6
6.3
7.1
8.0
9.0
MICROCOPY RESOLUTION TEST CHART
NATIONAL BUREAU OF STANDARDS - 1963 - A

FG. A 8

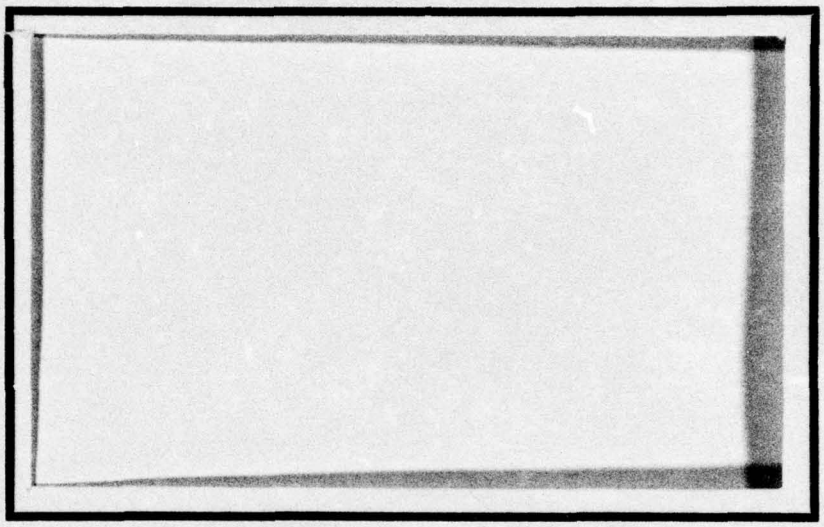

523,662

(3)

MICROWAVE DEVICE AND PHYSICAL ELECTRONICS LABORATORY DEPARTMENT OF ELECTRICAL ENGINEERING

UNIVERSITY OF UTAH
SALT LAKE CITY, UTAH 84112

523,662

This research was sponsored by
the Office of Naval Research
Contract No. N00014-67-A-0325-0005
Req. No. N00173-9-006132

(15)

(14) UTEC-MD-76-233

(6)

SOLID STATE OPTICAL DETECTOR

(9) Final Report - 1 Jun 71 - 30 Sep 74

For the Period

June 1, 1971 to September 30, 1974

by

(10) R. W. Grow, J. R. Boye, C. K. Peterson, and R. W. Ure, Jr.

August 27, 1976

(11) 27 Aug 76

(12) 101 p.

Microwave Device and Physical Electronics Laboratory
University of Utah
Salt Lake City, Utah 84112

229 550

bpg

ABSTRACT

A large area PIN silicon photodiode with a high quantum efficiency has been built and tested. The photodiode has an active window of diameter 200 μ, a microwave bandwidth from dc to 11 GHz, and has been optimized for use at 6328 Å. A unique Plesa guard-ring structure was employed to give near ideal breakdown voltage and internal gain. The photodiode was mounted in a microwave pill package at the end of a 2-Ω transmission line. A coaxial transformer provided a good match between the low series resistance of the photodiode (≃1 Ω) to a 50-Ω transmission line.

The 5145 Å line of a free-running argon ion laser was used as a source of "modulated" light since a 6328 Å source was not available. By beating the numerous longitudinal modes of the laser on the active surface of the photodiode, microwave frequencies from .115 GHz to 10.6 GHz at .115 GHz intervals could be observed and powers measured on a spectrum analyzer. A model for the photodiode and pill package along with a model for the free-running laser were derived, making it possible to predict the expected power output of the photodiode as a function of the parameters of the system. By comparing the experimental and predicted output curves, estimates of the parameters such as junction capacitance, lead inductance, quantum efficiency, and internal gain were made, which in turn were used to derive the frequency response of the photodiode. The parameters found were: a junction capacitance of 4 pF, internal gain of 2, and a quantum efficiency of 11 to 30 percent.

These parameters predict a photodiode bandwidth is in excess of 11.0 GHz. The bandwidth of the photodiode, pill package mounting system, and transformer was 4.2 GHz and was limited by the .75 nH lead inductance.

I. INTRODUCTION

With the development of the laser and its enormous bandwidth capabilities, the simultaneous development of the photosensing devices has proceeded. A photodiode is one of these devices and shows great promise due to its inherent sensitivity, ruggedness, and the ability to obtain large internal gain.[1] Because of this, many photodiodes have been built with responses into the microwave region. These devices have extremely small active areas and low quantum efficiencies, as with a point contact photodiode. This paper discusses the problems of building a large area high frequency photodiode and how they were overcome.

The theoretical considerations for using a free-running inhomogeneously broadened laser to obtain a millifrequency signal to test the photodiodes are discussed in some detail. These results have been used to obtain the frequency response of the photodiodes. The detailed description for the construction of the diode and the testing thereof are given in the appendices. The summary of these activities are presented as the text to provide an overview of how these various tasks were accomplished.

---

[1] L. K. Anderson and B. J. McMurthry, "High-Speed Photodetectors", *Proceedings of the IEEE*, Vol. 54, No. 10, October 1966, pp. 1335-1348.

II. PHOTODIODE DESIGN CONSIDERATIONS

In a semiconductor, a photon with energy greater than the band gap will produce a hole-electron pair when absorbed. The probability that a particular photon will be absorbed and produce an outside current is called the quantum efficiency, η. The equation that relates produced current to incident optical power is:

$$i(t) = \eta \frac{e\beta P_o(t)}{hf} \tag{1}$$

where e is the charge of an electron, β is the internal current gain, h is Planck's constant, f is the optical frequency, and $P_o(t)$ and i(t) are the optical power and current produced as a function of time.

For a photodiode, the diode and equivalent circuit are shown in Figs. 1 and 2.

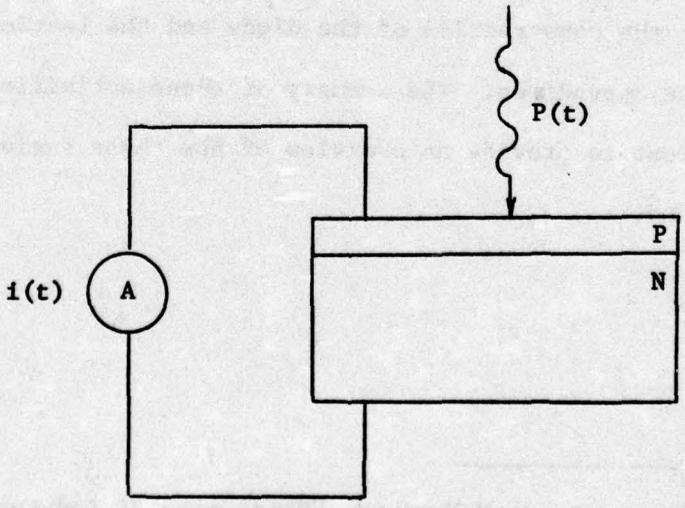

Fig. 1. Photodiode.

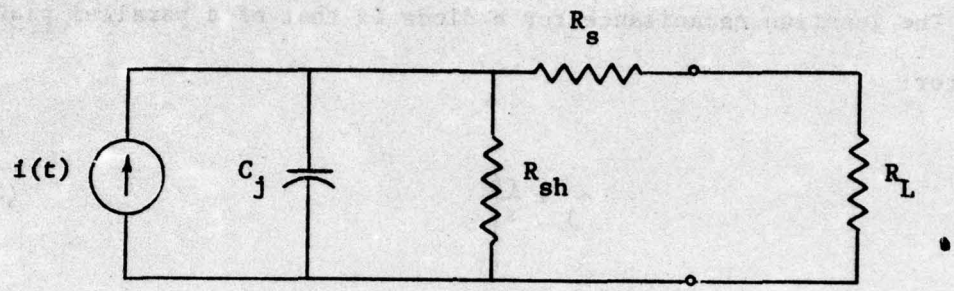

Fig. 2. Photodiode equivalent circuit.

For Fig. 2, the parameters are:

c_j -- the junction capacitance

i(t) -- the current generated

R_{sh} -- the shunt resistance

R_s -- the diode series resistance

R_L -- the load impedance

The cutoff frequency for the equivalent circuit of Fig. 2 for half power is[2]

$$f_{co} = \frac{1}{2\pi c_j \left(R_s + R_L\right)} \tag{2}$$

---

[2] Technical Report MDL-Q41, Microwave Device and Physical Electronics Laboratory, University of Utah, Salt Lake City, Utah, June 30, 1972, pp. 66-73.

where it has been assumed that $R_{sh} >> R_L + R_s$. The shunt resistance R_{sh} is usually 10^4 to 10^8 ohms, and $R_s + R_L$ is usually $\leq 50\ \Omega$.[3]

The junction capacitance for a diode is that of a parallel plate capacitor:

$$c_j = \frac{\varepsilon A}{x_j} \tag{3}$$

where ε is the dielectric constant of the medium, A is the area, and x_j is the depletion region width. It can be seen from Eqs. 2 and 3 that by making x_j as large as possible, the cutoff frequency, f_{co}, will be as large as possible for a given area. It is also obvious that for light-gathering considerations, A should be as large as possible. The limitation on x_j comes from transit time effects.

The depletion region of a photodiode can be treated as a planar diode. For a planar diode as shown in Fig. 3, the output current is:

$$i(t) = \sum_i \frac{q_i V_i}{x_j} \tag{4}$$

where the summation is over all charges in the depletion region, q_i is the ith carrier's charge, V_i is the ith carrier velocity, and x_j is the width of the depletion region.

For a charge injected into the planar diode at x = 0, t = 0,

---

[3] M. A. Riches, *Photodiodes*, Master's thesis, University of Utah, Salt Lake City, Utah, June 1972.

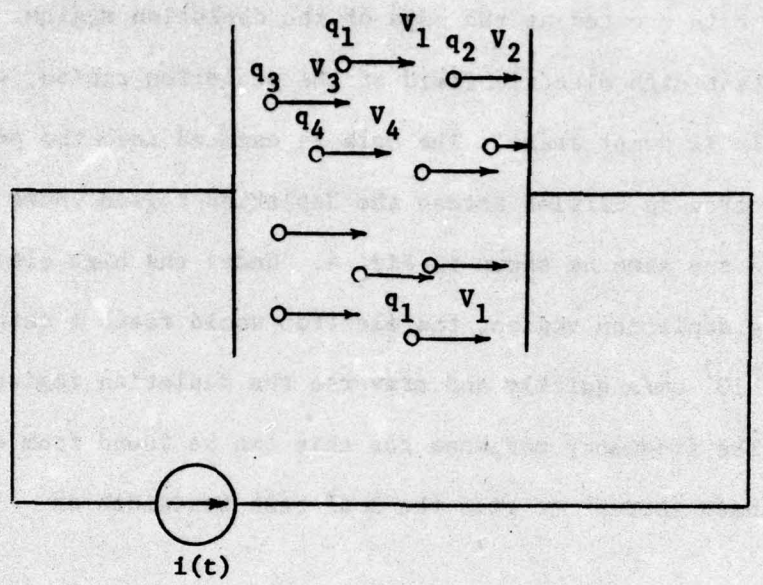

Fig. 3. Planar diode.

with constant velocity V and charge e, the output current will be as shown in Fig. 4, where $T = x_j/V$. This is the same as when a hole-

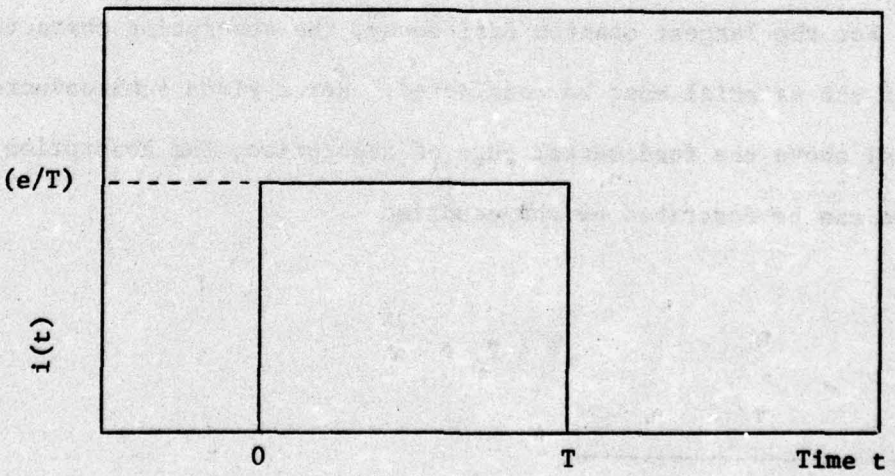

Fig. 4. Diode output current.

electron pair is created at the edge of the depletion region. In the nearly constant high electric field of the depletion region, the hole-electron pair is swept apart. The hole is carried into the p-region, and the electron is carried across the depletion region where the current will be the same as shown in Fig. 4. Under the high electric field of the depletion region, the electron would reach a saturation velocity of 10^7 cm/s quickly and traverse the depletion region at that velocity. The frequency response for this can be found from a simple Fourier transformation[4] to give the 3 dB base bandwidth as

$$\text{B.W.} = \frac{(0.445)V}{x_j} \tag{5}$$

This equation is in contradiction to Eqs. 2 and 3. It states that for a large bandwidth, the junction width must be small. Equations 2, 3, and 5 then define the parameters for a photodiode.

For the largest quantum efficiency, the absorption characteristics of the material must be considered. For a given semiconductor material above the fundamental edge of absorption, the absorption of photons can be described by the equation

$$P = P_o e^{-\alpha_1 x} \tag{6}$$

---

[4] M. DiDomenico, Jr. and O. Svelto, "Solid-State Photodetection: A Comparison between Photodiodes and Photoconductors", *Proceedings of the IEEE*, Vol. 52, 1964, pp. 136-144.

where P is the optical power at x, P_o is the incident power, α_1 is the absorption coefficient, and x is the distance into the material. Of the total incident photons, only those absorbed in the depletion region will contribute to the current. This is not strictly true, and some carriers generated near the edge of the depletion region may diffuse into the depletion region and contribute to the current. At high frequencies, this current is small due to the diffusion time involved and will be neglected.

For silicon, the absorption characteristics at some laser lines are given in Table 1.

Table 1. Absorption coefficient, α, for silicon at some laser lines.

Laser Wavelength	4545 Å	5145 Å	6328 Å
α_1 cm^{-1}	2×10^4	9×10^3	3.9×10^3

III. PHOTODIODE DESIGN

The photodiode as built is shown schematically in Figs. 5 and 6. The fabrication process involves sophisticated silicon technology. The masks are shown in Appendix II, with the step-by-step process given in Appendix I. The particular solutions used are given in Appendix III.

The design criteria as chosen are:

a. Bandwidth in excess of 11 GHz.

b. Active area window diameter of 200 μ.

c. Optimized for use at 6328 Å.

d. Series resistance in photodiode to be less than 1 Ω.

e. Diode to see an effective load impedance of 2 Ω.

f. Silicon to be used as the device material.

g. Large contact area on photodiode for mounting numerous leads to minimize lead inductance.

To meet these requirements and those of Eqs. 2, 3, and 5, a silicon PIN diode was built. A PIN diode minimizes the series resistance in the substrate and yet allows for the low concentration of carriers needed to give the large junction width. The wafers were obtained from Semimetals, Inc., of California. The wafers are <111> silicon, 1.5" in diameter by 5 mils thick. They are N on N^+, with a 5.5 Ω-cm epitaxial layer. The epitaxial layer has an average thickness of 7.4 μm. The substrate is antimony doped and has an average resistance of 0.01 Ω-cm.

The junction width was chosen to be 4 μm with a junction depth

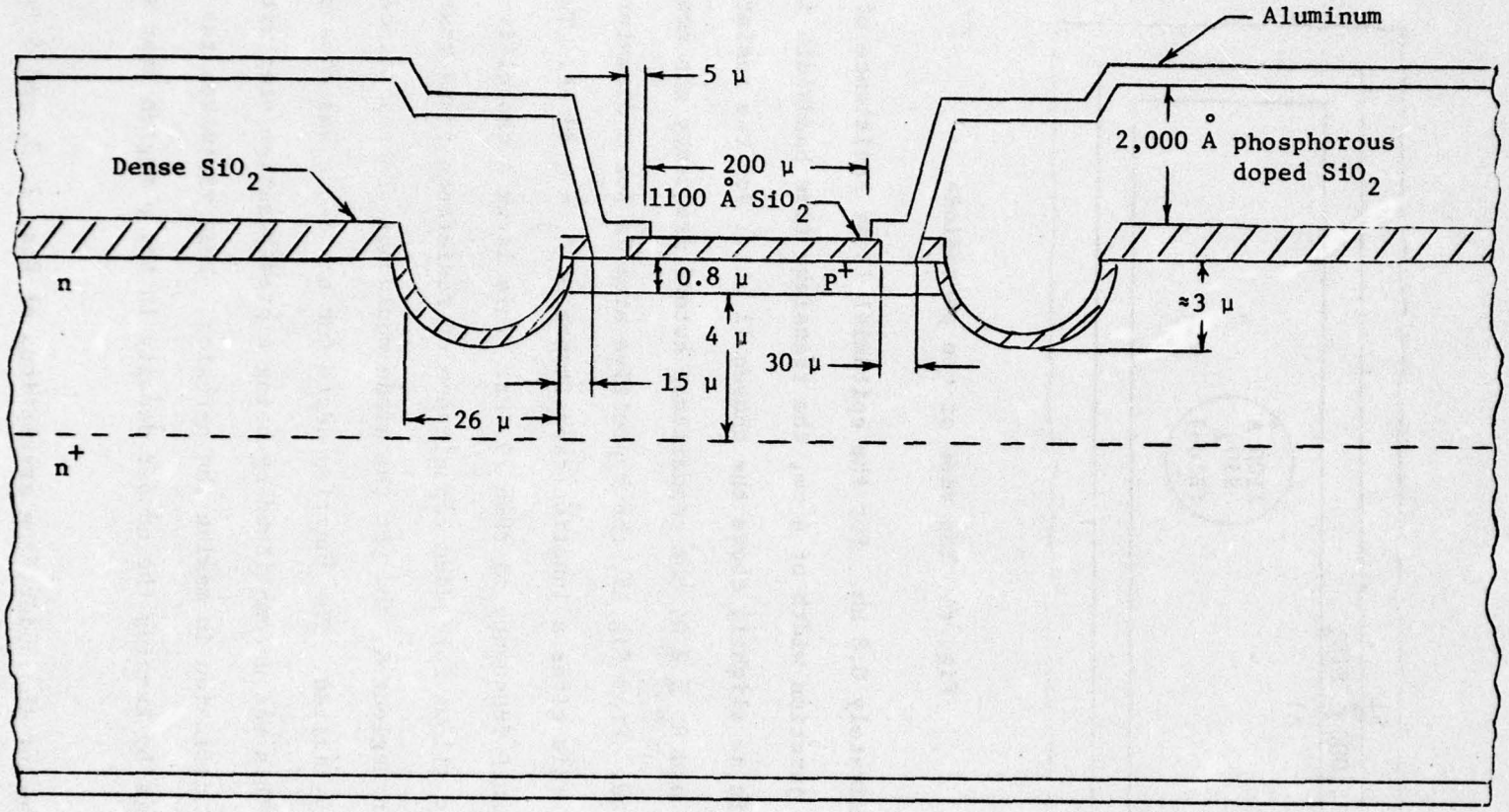

Fig. 5. Schematic representation of the photodiode.

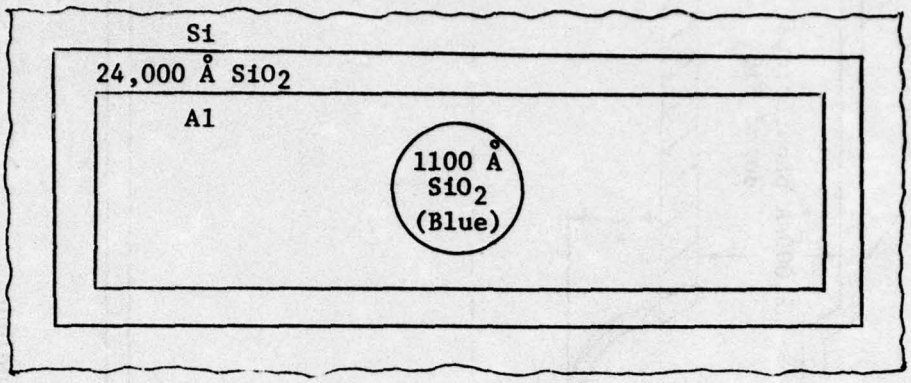

Fig. 6. Top view of the photodiode.

of approximately 0.8 μm. For the epitaxial layer resistance of 5.5 Ω-cm and a junction width of 4 μm, the transient time bandwidth is 11.125 GHz. This is slightly above the chosen 11 GHz. For the resistances of $R_s \leq 1\ \Omega$ and $R_L \simeq 2\ \Omega$, the capacitance cutoff frequency can now be calculated. From Fig. 5, the capacitive area is for a diameter of 300 μm. This gives a junction capacitance of $c_j = 1.83$ pF. The capacitive cutoff frequency is then 29 GHz. This large a capacitive cutoff frequency allows for added capacitance or resistance terms that may have been neglected, and yet the diode would not be capacitance cutoff frequency limited. The junction depth for the diode was chosen to be .8 μm. This was accomplished by using a predeposition step with no drive-in diffusion in making the p-region. This minimizes the series resistance by keeping the number density in the p region near saturation level.

One of the underlying assumptions of Eqs. 2, 3, and 5 is that

any desired junction width can be obtained. This is not true and unless special precautions and design considerations are made, a junction depth of 0.8 μm will have a maximum junction width[5] of 2 μm. If the voltage is increased to increase the junction width above 2 μ, edge breakdown will occur from junction curvature effects.[6] Decreasing the junction width below the 4 μm allowed by Eq. 5 decreases the quantum efficiency and minimizes the active area size. To design around this, a guard-ring is used.[7,8]

The usual guard-ring is a region of low impurities diffused into the diode at the edge of the junction. It has a low impurity gradient and sufficiently large radius of curvature that the central region will break down first. The limitation with using a guard-ring is that the added junction capacitance will be large and thereby limit the capacitive cutoff frequency. To design around this, a unique guard-ring was used.

The guard-ring structure used is a variation of the Varian Plesa structure. It can be seen in Fig. 5 as the small ring that circles the junction. The guard-ring was made by using a Si_3N_4 mask in the device

---

[5] A S. Grove, *Physics and Technology of Semiconductor Devices*, John Wiley and Sons, New York, 1967, pp. 163 and 197.

[6] *Ibid.*

[7] R. D. Baertsch, "Noise and Ionization Rate Measurements in Silicon Photodiodes", *IEEE Transactions on Electron Devices*, Vol. ED-13, 1966, p. 987.

[8] H. Melchior and W. T. Lynch, "Signal and Noise Response of High Speed Germanium Avalanche Photodiodes", *IEEE Transactions on Electron Devices*, Vol. ED-13, 1966, p. 829.

fabrication. The Si was then etched away with a silicon etch (see Appendix III). A dense 2000 Å SiO_2 layer was then grown on the bare Si quickly after the Si etching. The SiO_2 layer was grown at high temperature to limit any "piling up" of the epitaxial dopent at the Si-SiO_2 surface.[9] The Si_3N_4 is then removed. The removal of the Si_3N_4 acts as a self-aligning mask for the boron diffusion. The boron (p-region) is then diffused into the Si. The SiO_2 over the guard-ring then acts as a barrier for the boron being diffused into the Si. This keeps the doping profile nearly flat across the width of the junction. The breakdown voltage will then be near ideal.

To minimize optical reflection as the light enters the active area, an 1100 Å thick SiO_2 quarter-wave optical antireflection coating was added. This minimizes reflection for normal incident light to 7.9 percent at 6328 Å and 12.8 percent at 5145 Å.

In mounting the photodiode, a large area for making contact is required. This was apparent since calculations showed that if a single 0.5 mil wire were used in mounting, the inductance from the wire would be high.[10] To minimize this problem, large "wings" were added to the sides of the photodiode (see Fig. 6). They would allow the use of six or more wires in making contact. It was hoped that this would minimize the problem of the inductance.

---

[9] A. S. Grove, *Physics and Technology of Semiconductor Devices*, John Wiley and Sons, New York, 1967, pp. 69-75.

[10] *Microwave Engineers Handbook*, Artech House, Inc., Dedham, Massachusetts, Vol. 1, 1971, pp. 100-102.

In operating the photodiode, a large reverse bias is applied. For our design, an operating voltage of around 120 volts theoretical is required. This required a thick layer of SiO_2 on top of the photodiode and under the contact wings to eliminate the formation of an inversion layer underneath the mounting wings. For the diode, 20,000 Å of phosphorous-doped SiO_2 was used. The inversion layer would add a large capacitance to the junction capacitance and drop the capacitance cutoff frequency by approximately two orders of magnitude.

IV. PHOTODIODE TESTING

In order to handle the photodiode, it is mounted in a microwave "pill" package made by Fansteel Ceramics International of New Jersey. The package is shown in Fig. 7 and is made of gold-plated kovar and

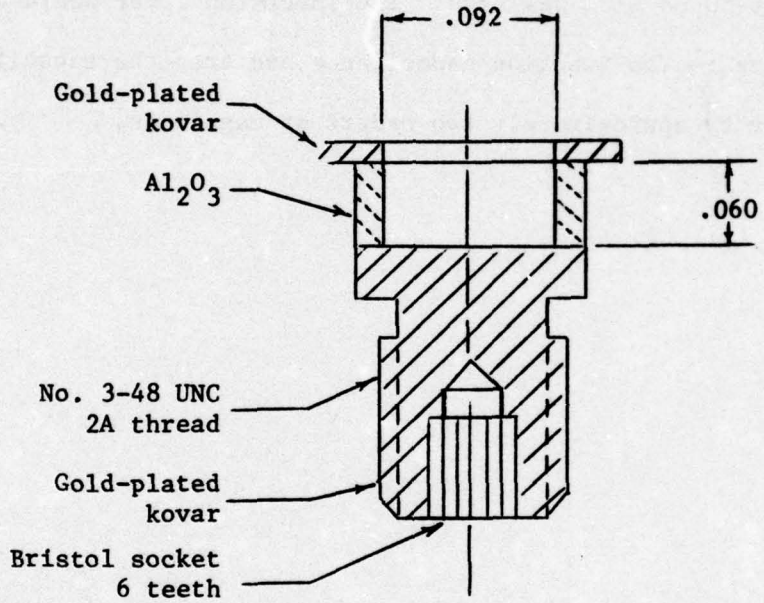

Fig. 7. Microwave "pill" package.

alumina ceramic. The mounting capacitance from the "pill" package is three orders of magnitude less than the junction capacitance, and is neglected.

The photodiode is mounted in the "pill" package with standard silicon device technology. The mounting involves heating the "pill"

package to 435°C. A small amount of Au-Si solder is then placed in the bottom center of the "pill" package. As soon as the solder wets the gold, the photodiode is placed in the "pill" package and, with a pair of tweezers, scrubbed against the bottom until a good mechanical and electrical contact has been made. The "pill" package and photodiode are then cooled and placed in the wire bonder. A standard 0.5 mil gold wire bonder is then used and 7 or 8 wire bonds are made from the photodiode "wings" to the top of the "pill" package. If a good mechanical contact between the diode and "pill" package has not been made, the diode will usually lift off of the "pill" package at that time.

To obtain the desired cutoff frequency, the load impedance must be approximately 2 ohms. It must also appear as 2 ohms over a wide frequency range. To accomplish this, a 2-ohm characteristic impedance coaxial line was built. For use with standard equipment, this was then transformed to a 50-ohm characteristic impedance. This was accomplished by using a Gaussian transformer. For a Gaussian transformer, the characteristic impedance, z_o, varies smoothly between $x = \pm\infty$ according to Gaussian law:[11]

$$\frac{d \ln z_o(x)}{dx} = k\, e^{-h^2 x^2} \qquad (7)$$

where k and h are constants. In practice, the line must have a finite

---

[11] A. D. Lewis and F. H. Wells, *Millimicrosecond Pulse Techniques*, Pergamon Press, New York, pp. 74-114.

length, say 2 ℓ, and the distribution is accordingly Gaussian over this range only. Letting z_1 and z_2 be the impedance between which you are to transform, then

$$z_o(x) = z_1 \quad \text{for} \quad x \leq -\ell \tag{8}$$

and

$$z_o(x) = z_2 \quad \text{for} \quad x \geq +\ell \tag{9}$$

When these conditions are applied to the integral of Eq. 7 between the limits of $\pm\ell$, you obtain

$$\ln \frac{z_o(x)}{z_1} = \frac{1}{2} \ln \frac{z_2}{z_1} \left[1 + \frac{\text{erf } (hx)}{\text{erf } (h\ell)}\right] \tag{10}$$

For the chosen load impedance of 2 ohms, a coaxial system was chosen. The dielectric medium between the inner and outer conductor is teflon, with a relative dielectric constant of $\varepsilon_r = 2.1$. For ease in construction, the inner conductor of the coaxial system was chosen to be constant with a diameter of 1/8 inch. The length of the transforming section between the 2-ohm and the 50-ohm characteristic impedance was 2.5 inches. Calculations show that this will work well over the frequency necessary.

For a coaxial line, the characteristic impedance z_o is given by

$$z_o = \frac{\mu}{\varepsilon} \frac{\ln(b/a)}{2\pi} \qquad (11)$$

where μ and ε are the permeability and permittivity of the insulation material between the inner and outer conductors, and a and b are the inner and outer diameters of the conductors, respectively. The designed transformer was built for an $h\ell$ product of 2.0. A length 2ℓ = 2.5 inches, and an inner diameter of 0.125 inch, were also chosen. The impedances z_1 and z_2 were chosen as before to be 50 ohms and 2 ohms, respectively. With these parameters, values of b as a function of x were calculated. The results are shown in Table 2.

Table 2. Characteristic impedance and dimensions versus x for coaxial Gaussian line transformer.

x_o (inches)	$Z_o(x)$ (ohms)	a (inch)	b (inch)
-1.25	50.000	.125	.418
-1.00	48.489	.125	.403
-0.875	46.635	.125	.385
-0.750	43.573	.125	.358
-0.625	39,062	.125	.321
-0.500	33,198	.125	.278
-0.375	26,547	.125	.237
-0.250	19,9912	.125	.2025
-0.125	14,334	.125	.177
0	10.000	.125	.159
+0.125	6.9758	.125	.147
+0.250	5.0021	.125	.141
+0.375	3.7664	.125	.136
+0.500	3.0119	.125	.134
+0.750	2.29470	.125	.132
+1.00	2.06231	.125	.131
+1.25	2.0000	.125	.131

V. LIGHT MODULATION AND FREQUENCY RESPONSE

To test the photodiode, a high frequency modulated light beam was needed. Various schemes were tried but all proved infeasible.[12,13] We then obtained a high power Spectra-Physics argon-ion laser. By using the various longitudinal modes of the argon-ion laser at 5145 Å, mixing frequency components were formed by the photodiode. It was found that by using this scheme, frequences up to 10.4 GHz were observed.

For the argon-ion laser at 5145 Å, the laser output as might be observed is shown in Fig. 8.

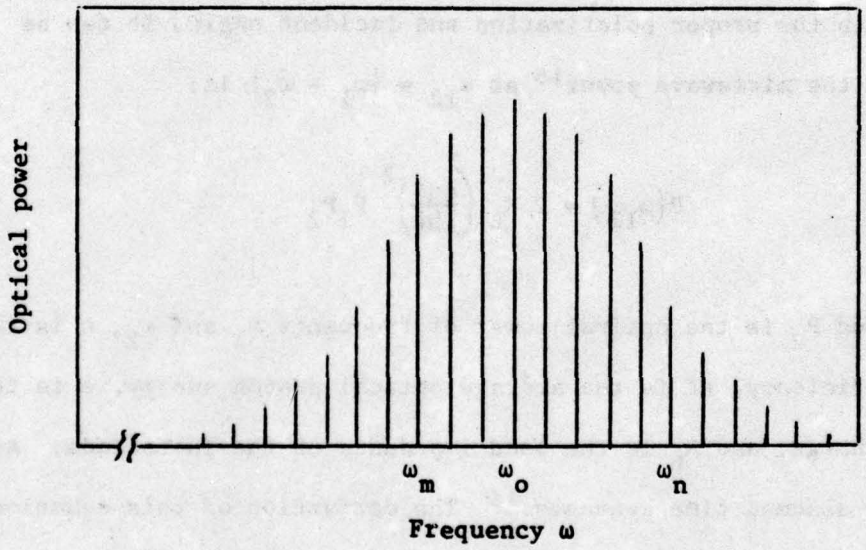

Fig. 8. Possible output of argon-ion laser with various longitudinal modes. The center frequency, ω_o, is for 5145 Å.

---

[12] Technical Report MDL-Q40, Microwave Device and Physical Electronics Laboratory, University of Utah, Salt Lake City, Utah, March 31, 1972, pp. 74-83.

[13] Technical Report MDL-Q50, Microwave Device and Physical Electronics Laboratory, University of Utah, Salt Lake City, Utah, September 30, 1974, p. 23.

The laser will operate in several modes at frequency ω_n with frequency spacing $\delta = c/2\,L$. The constant c is the speed of light, and L is the length of the laser cavity. The beat frequency between any of these modes can be observed with the photodiode, which is a square law detector. As an approximation, $\omega_n = n\delta$, where n is an integer on the order of 10^6. The beat frequency between the two modes[14] will be $\omega_{nm} = |n - m|\delta$. The difference between n and m is called ρ and is defined as $\rho = |n - m|$. With the argon-ion laser at 5145 Å and 2.4 watts continuous, the maximum ω_{nm} corresponds to approximately 10.4 GHz.

For the photodiode with two incident optical frequencies, ω_1 and ω_2, with the proper polarization and incident angle, it can be shown that the microwave power[15] at $\omega_{12} = |\omega_1 - \omega_2|$ is:

$$P(\omega_{12}) = 2\,R_L \left(\frac{e\eta\beta}{hf}\right)^2 P_1 P_2 \qquad (12)$$

where P_1 and P_2 is the optical power of frequency ω_1 and ω_2, η is the quantum efficiency, hf is the average optical photon energy, e is the electron charge, and R_L is the load impedance of the photodiode. All powers are assumed time averages.[16] The derivation of this equation

---

[14] W. R. Bennett, Jr., *Physical Review*, Vol. 126, April 15, 1962, pp. 500-593.

[15] D. Marcuse, lecture given at the University of Utah, October 22, 1971.

[16] J. R. Boye, *Method for Obtaining the Frequency Response of a Microwave Photodiode using an Inhomogeneously Broadened Laser*, Master's thesis, University of Utah, Salt Lake City, Utah, 1976.

is given in Appendix IV.

The photodiode-pill package-transformer as seen at the diode is shown in Fig. 9. An equivalent circuit for the photodiode-pill-trans-

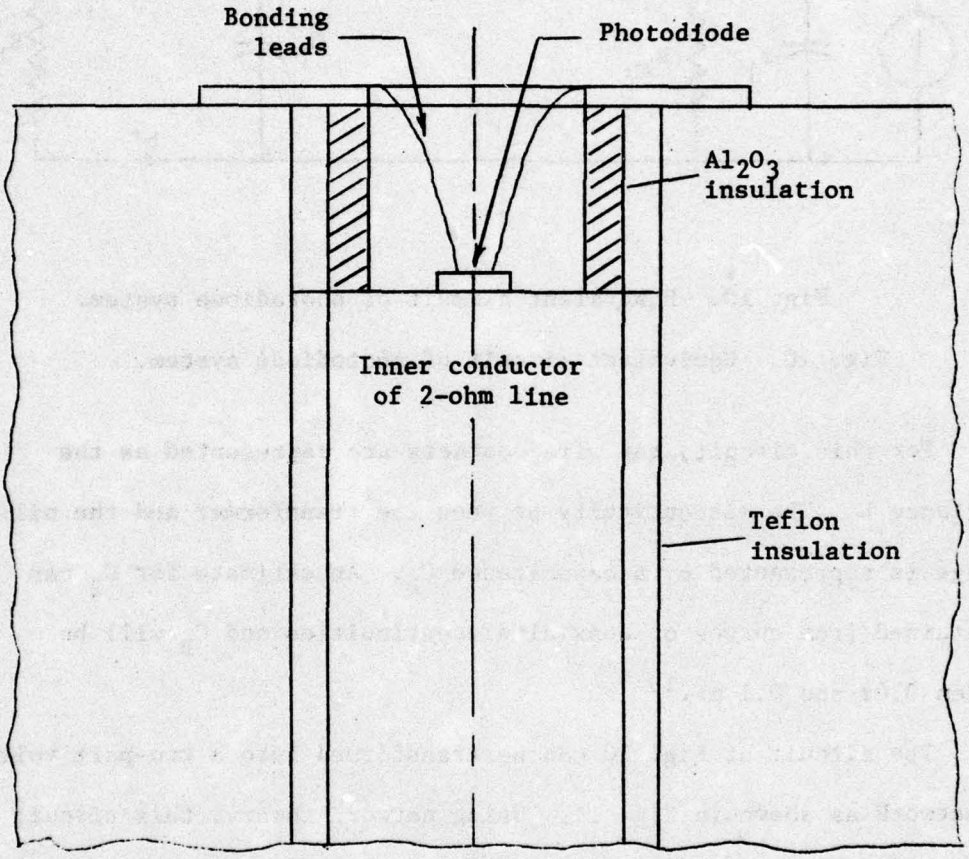

Fig. 9. Photodiode pill-package as mounted at the 2-ohm end of the transformer.

former system is needed in order to predict the expected power output as a function of frequency. An equivalent circuit that represents

this system[17] quite well is shown in Fig. 10.

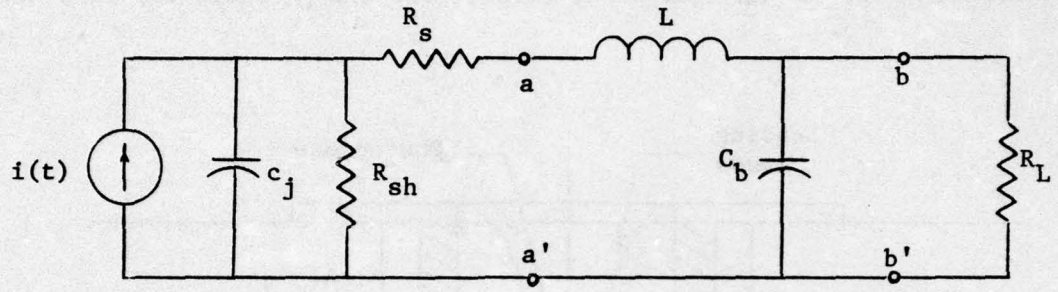

Fig. 10. Equivalent circuit of photodiode system.

Fig. 10. Equivalent circuit of photodiode system.

For this circuit, the wire contacts are represented as the inductance L. The discontinuity between the transformer and the pill package is represented by a capacitance C_B. An estimate for C_B can be obtained from curves on coaxial discontinuities and C_B will be between 0.02 and 0.1 pF.[18]

The circuit of Fig. 10 can be transformed into a two-port voltage network as shown in Fig. 11. Using network theory, this circuit can be solved for the frequency response of the total photodiode system. The power output as a function of the frequency, the circuit components, and the diode current as derived in Appendix V is then written:

---

[17] Ibid.

[18] *Microwave Engineers Handbook*, p. 111.

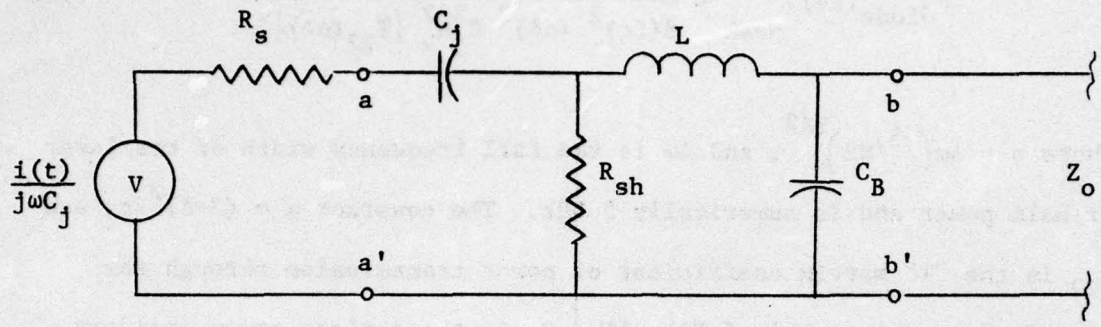

Fig. 11. Voltage equivalent circuit of photodiode.

$$\overline{P_o} = \frac{1}{8\omega^2 C_j R_s \left|T_{22}\right|^2} \left|I\right|^2 \tag{13}$$

The diode current I in terms of the incident light is derived in Appendix VI, and a discussion of mode coupling effects on the observed output is discussed in Appendix VII.

The procedure of using the mixed components of a free running inhomogeneously broadened laser to measure the frequency response of a photodiode has not previously been reported. Some of the data obtained are given in Appendix VIII, and the experimental procedure for making the measurements is discussed in Appendix IX. As based on these and the confidence gained in being able to understand the laser processes and predict their effect on the signal applied to the photodiode, the expected diode output using the equivalent circuit of Fig. 11 is then[19]

$$P_{diode}(\rho\delta)\Big|_{peak} = \frac{(\sqrt{2}\,\eta\beta e/hf)^2\, P_o^2\, e^{-\alpha\,\rho^2/2}}{8(2\pi)^2\,(\rho\delta)^2\, C_j^2 R_s^2\, |T_{22}(\rho\delta)|2} \qquad (14)$$

where $\sigma = \Delta\omega\left(2^3/N2\right)^{\gamma/2}$, and $\Delta\omega$ is the full frequency width of the laser at half power and is numerically 5 GHz. The constant $\alpha = (2\pi\delta)^2 2\sigma$, and T_{22} is the "T" matrix coefficient of power transmission through the circuit from aa' to bb' of Fig. 11. P_o is the optical power incident upon the active area of the photodiode. Rewriting Eq. 14 in dBm gives

$$10\,\log_{10}\left[\overline{P_{diode}}(\rho\delta)\Big|_{peak}\right] = 20\,\log_{10}\sqrt{2}\,\eta\beta$$

$$+ 10\,\log_{10}\left[\left\{8(2\pi)^2(\rho\delta)^2 C_j^2 R_s^2 |T_{22}(\rho\delta)|^2\right\}^{-1}\right]$$

$$+ 10\,\log_{10}\left[(e/hf)^2\, P_o^2\, e^{-\alpha\,\rho^2/2}\right] + 30 \qquad (15)$$

The first term in Eq. 15 separates out the quantum efficiency. The second term is proportional to the attenuation introduced from the mismatch between the photodiode and the matching circuit. The third term is the power from the laser. It has been assumed that the laser line shape is Gaussian.[20,21]

---

[20] J. R. Boye, *op. cit.*

[21] A. E. Siegman, *An Introduction to Lasers and Masers*, McGraw-Hill Book Company, Inc., New York, 1971, Chapter 9.

VI. PHOTODIODE RESPONSE AND QUANTUM EFFICIENCY

Direct current measurements were made on the photodiodes. The dark current breakdown of the diodes was between 80 and 110 volts. The dark current was less than 0.1 μA at 5 volts below the breakdown voltage. The breakdown voltage is extremely sharp for low optical incident powers. The observed breakdown voltages predict junction widths of 2.66 μ to 3.66 μ. This is less than the designed junction width of 4 μ. This predicts that the transit time limiting effect would be negligible for the chosen bandwidth of 11 GHz. The calculated junction capacitance for the observed breakdown voltages is between 2.0 and 2.75 pF. For these capacitances, the cutoff frequency from the junction capacitor is not a limiting factor at 11 GHz.

The frequency response of the photodiode was measured with the argon-ion laser tuned to 5145 Å at 2.4 watts continuous total laser power output. Of this power, 6 mW was incident upon the active area of the photodiode. The predicted response of the photodiode in terms of the frequency and the parameters of the equivalent circuit is given in Appendix X. The response as measured with a spectrum analyzer is shown in Fig. 12. The measurements were made in both the S and X frequency bands. At each frequency, the spectrum analyzer was calibrated against a known power source. The reading taken was the average peak power as observed on the spectrum analyzer. Power readings up to 9.66 GHz were taken, with frequencies of up to 10.45 GHz observed.

The dc quantum efficiency was found by first observing the gain β.

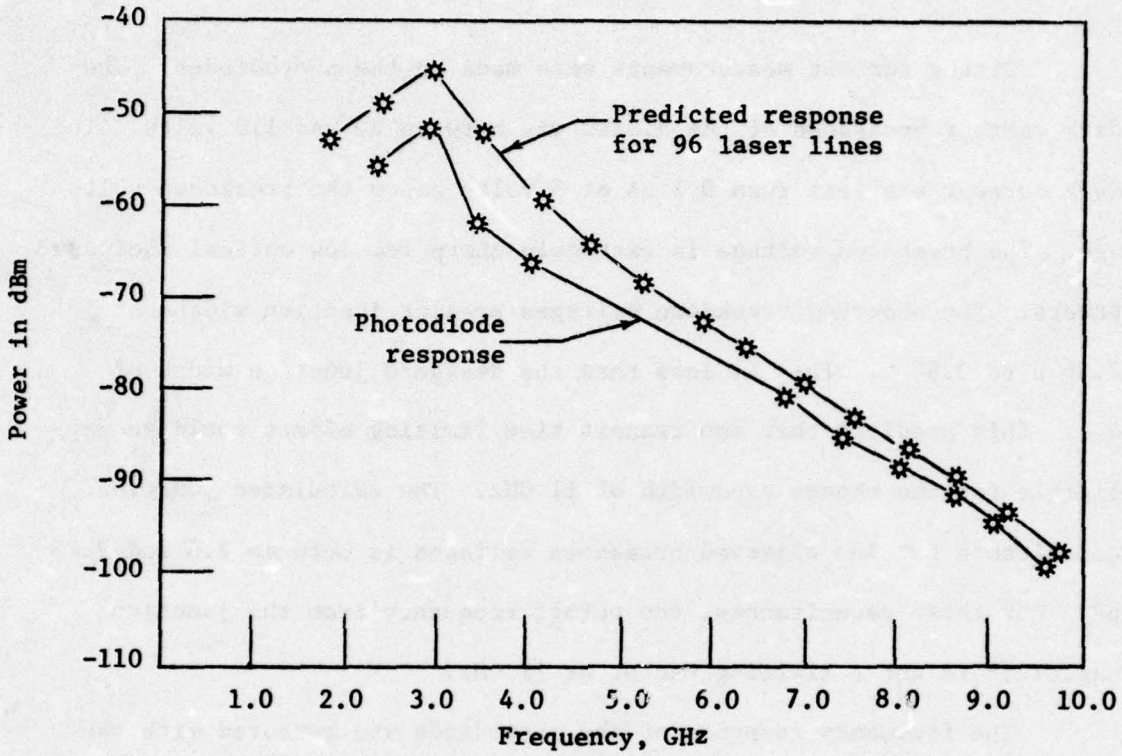

Fig. 12. Measured and predicted response of the photodiode for 5145 Å argon-ion laser light. The optical power on the active area of the photodiode is 6 mW.

The gain was observed by using a transistor curve tracer which displays voltage versus current characteristics. The incident optical power on the active area of the photodiode was 6 mW. The transistor curve tracer was hooked up to the photodiode system. The bias voltage was then increased and the current increased until it reached a plateau of 2 mA. The plateau indicated that the depletion region had reached its maximum width. The voltage was then doubled with no visible increase in the current. The voltage at this point was approximately 40 volts.

The voltage was then increased to approximately 85 volts with an apparent exponential increase in current to 4 mA. This is the bias at which the photodiode was operated, giving the current gain as 2. Equation 1 then gives the dc quantum efficiency as 63.2 percent at 5145 Å.

The predicted response from Eq. 15 is shown on Fig. 12. The parameters used are:

$$C_j = 4 \text{ pF}$$
$$R_s = 1 \text{ ohm}$$
$$Z_o = 2 \text{ ohms}$$
$$L = 0.75 \text{ nH}$$
$$C_B = 0.02 \text{ pF}$$

The upper curve of Fig. 12 is a plot of Eq. 15 with $\sqrt{2}\ \eta\beta = 1$ chosen as a reference. The difference between the two curves is 2 to -10 dBm, or

$$20 \log_{10} \sqrt{2}\ \eta\beta = 0 \text{ to } -6 \qquad (16)$$

or the quantum efficiency is, for $\beta = 2$,

$$\eta = 11 \text{ to } 30 \text{ percent} \qquad (17)$$

The evaluation of the quantum efficiency is described in Appendix XI.

The fit between the predicted results and the measured curve is good. The curve fitting of $C_j = 4$ pF is close to the calculated junction capacitance of 2.0 pF to 2.75 pF. The curve fitted capacitance

of 4 pF is probably closer to the actual junction capacitance than the calculated capacitance since the calculated capacitance neglects fringing capacitance. The assumed resistances of R = 1 ohm and the calculated resistance of R_L = 2 ohms appear to be correct. The capacitance C_B = 0.02 pF appears to be correct.

A great deal has been assumed about the laser and its output. In calculating the laser output, a Gaussian broadening has been assumed and mode competition has been completely ignored. If mode competition has an appreciable effect, it will lower the possible laser output and thereby raise the calculated quantum efficiency. If mixed frequencies do not occur in pairs as expected, the predicted laser output would again be lowered and the calculated quantum efficiency increased. The predicted curve shape is also less dependent on the laser than on the circuit parameters of the photodiode system. The shape of the curve depends almost completely on the value of the lead inductance and the junction capacitance. The tail of the predicted curve is sensitive to the parameter α, but the curve dependence on the inductance, L, is much greater. The effect of reflection caused by the coaxial transformer has been neglected and could change the shape of the curve, but considering the effect of the inductance, L, and the overall good fit, the effect of the transformer seems to be small.

The shape of the predicted curve depends chiefly on the effective diode circuit parameters and mounting circuit, and little on the uncertainties of the laser. A comparison of the experimental and predicted curves gives a good basis for deciding if the model and circuit

actually represent the system. Inspection of Fig. 12 clearly indicates that the circuit model with R_s = 1 ohm, Z_o = 2 ohms, C_j = 4 pF, C_B = 0.02 pF, $R_{sh} = 10^3$ ohms, and L = 0.75 nH closely represents the actual circuit.

VII. CONCLUSION

It is apparent from Fig. 12 that the photodiode as built has an excellent quantum efficiency and frequency response. It is also apparent that the response of the photodiode system is limited by the inductance of the bonding leads. From the observed breakdown voltage and the calculated capacitance and transit time cutoff frequencies, it is apparent that the cutoff frequency of the photodiode is greater than 11 GHz.

The frequency response could be improved by reducing the lead inductance. A lead inductance of ~0.05 nH would cause the peak in the response curve to occur at 12 GHz instead of 3 GHz and actually give a rising frequency response as 12 GHz is approached from below. The quantum efficiency of the diode appears to be on the order of 32 to 67 percent; however, the accuracy seems to be in some doubt.

The general scheme of using the longitudinal modes of a laser as sources of modulated light appears to work well in the present situation. While the absolute placement of the predicted curves was left in some doubt, the uncertainties concerning the laser output had little effect on the overall prediction of the frequency response.

APPENDIX I

DEVICE FABRICATION PROCESS

1. Standard cleanup cycle
   a. Etch in hot chromic acid (95-105°C) for 15 minutes
   b. Hot water bath and deionized water rinse
   c. Deionized water spray rinse and spin dry
   d. Dip in 1:10 $HF:H_2O$ for 10 seconds to dewet
   e. Deionized water spray rinse and spin dry

   (Steps d and e immediately before going to next step)
2. Outdiffuse and oxidize (grow ~6000 Å of SiO_2)
   a. Anneal 16 hours in dry O_2 at 1100°C
3. Photostep, mask No. 1
   a. Apply Waycoat Photoresist. Spin for 30 seconds at 4000 rpm
   b. Bake 15 minutes 110°C
   c. Expose through mask No. 1 for 2 seconds
   d. Develop by spraying: 30 seconds Stoddard solvent
      20 seconds n-butyl acetate
   e. Inspect
   f. Bake 20 minutes at 150°C
4. Oxide etch
   a. Place wafers in basket at oxide etch station
   b. Etch in oxide etch to dewet for 6 minutes nominal
   c. Deionized water dip rinse
   d. Deionized water spray rinse and spin dry

5. Strip photoresist

   a. Etch in hot chromic acid (95-105°C) for 15 minutes

   b. Hot water rinse and deionized water rinse

   c. Deionized water spray rinse and spin dry

   d. Dip in 1:10 HF:H_2O for 10 seconds to dewet

   e. Deionized water spray rinse and spin dry

   (Steps d and e immediately before going to next step)

6. Grow 100-200 Å oxide

   a. Five minutes in dry O_2 at 950°C

   b. Measure thickness by measurement of breakdown voltage using transistor curve tracer

7. Deposit 500 Å of Si_3N_4

   a. $SiCl_4$ + NH_4 in N_2 carrier at 1000°C using standard 5-7-5 minute cycles

      Flush with N_2 for 5 minutes

      $SiCl_4$ + NH_4 in N_2 carrier for 7 minutes

      Flush with N_2 for 5 minutes

   b. Measure thickness by measurement of breakdown voltage using transistor curve tracer

8. Deposit 1000 Å SiO_2 by pyrolytic decomposition of silane

   a. Set temperature of rotating hot plate at 800°F

   b. Place wafers on rotating hot plate and flush system with N_2

   c. Start silane (SiH_4) and O_2

   d. Grow 1000 Å SiO_2 (approximately 2 minutes)

   e. Determine thickness by color

9. Densify SiO_2

   a. Bake at 950°C in dry O_2 for 5 minutes

10. Photostep, mask No. 2

   a. Apply Waycoat Photoresist, Spin for 30 seconds at 4000 rpm

   b. Bake 15 minutes at 110°C

   c. Expose through mask No. 2 for 2 seconds

   d. Develop by spraying: 30 seconds Stoddard solvent
      20 seconds n-butyl acetate

   e. Inspect

   f. Bake 20 minutes at 150°C

11. Oxide etch

   a. Place wafers in basket at oxide etch station

   b. Etch in oxide etch for 2 minutes nominal

   c. Deionized water dip rinse

   d. Deionized water spray rinse and spin dry

12. Strip photoresist

   a. Etch in hot chromic acid (95-105°C) for 15 minutes

   b. Hot water rinse and dionized water rinse

   c. Dionized water spray rinse and spin dry

   d. Dip in 1:10 $HF:H_2O$ for 10 seconds to dewet

   e. Deionized water spray rinse and spin dry

   (Steps d and e immediately before going to next step)

13. Nitride etch

   a. Etch in phosphoric acid (H_3PO_4) boiling at 180°C for 5 minutes nominal

b. Hot water bath

c. Deionized water spray rinse and spin dry

14. Oxide etch

a. Place wafers in basket at oxide etch station

b. Etch in oxide etch to dewet for 2 minutes nominal. The dewet may be difficult to see

c. Deionized water dip rinse

d. Dionized water spray rinse and spin dry

15. Silicon etch

a. Dissolve black wax in TCE (trichloroethylene)

b. Swab on rear of wafer with Q-tip

c. Heat wafer on hot plate to drive off TCE

d. Etch wafer in silicon etch for 10 minutes to get a 2 μm etch depth

e. Check etch depth with interferometer

f. Remove wax with TCE

16. Standard cleanup cycle

a. Etch in hot chromic acid (95-105°C) for 15 minutes

b. Hot water rinse and deionized water rinse

c. Deionized water spray rinse and spin dry

d. Dip in 1:10 $HF:H_2O$ for 10 seconds to dewet

e. Deionized water spray rinse and spin dry

(Steps d and e immediately before going to next step)

17. Oxidation, grow 2000 Å of SiO_2

a. Anneal at 1100°C for 10 minutes in wet O_2

b. Anneal at 1100°C for 20 minutes in dry O_2

18. Etch oxide over Si_3N_4 (must be short etch so oxide over grooves is not removed)

a. Place wafers in basket at oxide etch station

b. Etch in oxide etch for 20 seconds nominal

c. Dionized water dip rinse

d. Deionized water spray rinse and spin dry

19. Nitride etch

a. Etch in phosphoric acid (H_3PO_4) boiling at 180°C for 5 minutes nominal

b. Hot water dip

c. Deionized water spray rinse and spin dry

20. Oxide etch

a. Place wafers in basket at oxide etch station

b. Etch in oxide etch to dewet for 20 seconds nominal

c. Deionized water dip rinse

d. Deionized water spray rinse and spin dry

21. Diffuse boron for a 1 μm junction depth

a. Diffuse boron in a standard predeposition cycle of 5-9-5 minutes at 1070°C to give a sheet resistance of 13 ohms

22. Remove B-doped glass

a. Etch in boron glass etch for 2 minutes

b. Deionized water rinse

c. Deionized water spray rinse and spin dry

23. Deposit thick (~20,000 Å) phosphorous-doped SiO_2

    a. Check time for steps d and f below by running a test wafer first. Determine the SiO_2 thickness by weighing test wafer here and after step 23F.

    b. Set temperature of rotating hot plate at 800°F

    c. Place wafers on rotating hot plate and flush system with N_2

    d. With N_2 flowing, start silane (SiH_4) and O_2. Grow 1000 Å of oxide (approximately 2 minutes)

    e. Turn on Phosphene (PH_3)

    f. Grow total depth of 20,000 Å of SiO_2 (approximately 20-40 minutes)

24. Densify SiO_2

    a. Anneal at 950°C for 10 minutes in N_2 with small addition of HCl (HCl purifies the surface and stabilizes MOS threshold)

    b. Determine SiO_2 thickness by weighing hot wafer

25. Photostep, mask No. 3

    a. Apply Waycoat Photoresist. Spin for 30 seconds at 4000 rpm

    b. Bake 15 minutes at 110°C

    c. Expose through mask No. 3 for 2 seconds

    d. Develop by spraying: 30 seconds Stoddard solvent
       20 seconds n-butyl acetate

    e. Inspect

    f. Bake 20 minutes at 150°C

    May have trouble with photoresist sticking

26. Etch Phosphene-doped SiO_2

    a. Etch in diluted oxide etch 2:1 oxide etch, water to dewet 8 minutes nominal

    b. Deionized water dip rinse

    c. Deionized water spray rinse and spin dry

27. Strip photoresist

    a. Etch in hot chromic acid (95-105°C) for 15 minutes

    b. Hot water rinse and deionized water rinse

    c. Deionized water spray rinse and spin dry

    d. Dip in 1:10 $HF:H_2O$ for 10 seconds to dewet

    e. Deionized water spray rinse and spin dry

    (Steps d and e immediately before going to next step)

28. Grow 1100 Å SiO_2

    a. Anneal at 950°C in wet O_2 for 12-15 minutes

    b. Switch to N_2 at high flow rate for 5 minutes

29. Photostep, mask No. 4

    a. Apply Waycoat Photoresist. Spin for 30 seconds at 4000 rpm

    b. Bake 15 minutes at 110°C

    c. Expose through mask No. 4 for 2 seconds

    d. Develop by spraying: 30 seconds Stoddard solvent
    20 seconds n-butyl acetate

    e. Inspect

    f. Bake 20 minutes at 150°C

30. Oxide etch

    a. Place wafers in basket at oxide etch station

b. Etch in oxide etch to dewet for 1.5 minutes nominal

c. Deionized water dip rinse

d. Deionized water spray rinse and spin dry

31. Strip photoresist

a. Etch in hot chromic acid (95-105°C) for 15 minutes

b. Hot water rinse and deionized water rinse

c. Deionized water spray rinse and spin dry

d. Dip in 1:10 $HF:H_2O$ for 10 seconds to dewet

e. Deionized water spray rinse and spin dry

(Steps d and e immediately before going to next step)

32. Clean

a. Etch in 10:1 $H_2O:HF$ to dewet

b. Deionized water rinse and spin dry

c. Go immediately to next step

33. Evaporate aluminum

a. Evaporate 7000-8000 Å of Al

b. Determine thickness by weighing test wafer

34. Alloy aluminum

a. Anneal at 440°C for 10 minutes in dry N_2

35. Photostep, mask No. 5

a. Apply Shipley Az 1350 H Photoresist. Spin for 20 seconds at 3000 rpm

b. Bake 15 minutes at 105°C

c. Expose through mask No. 5 for 10 seconds

d. Develop 1 minute

e. Deionized water spray rinse and spin dry

f. Inspect

g. Bake for 30 minutes at 150°C

36. Aluminum etch

a. Etch in commercial "green goddess" etch

b. Quench in dionized water

c. Inspect

37. Strip Photoresist

a. Acetone bath for 10 minutes nominal

b. Etch in commercial J-100 stripper for 5 minutes at 105°C

c. Rinse in xylene

d. Rinse in alcohol

e. Dionized water rinse and spin dry

f. Inspect

38. Back side etch

a. Place wafer face down on filter paper

b. With Q-tip, swab xylene over back side of wafer, dry

c. With Q-tip, swab HF over back side of wafer. Do not allow the HF to run over the edges of the wafer.

d. Quench etch in dionized water

e. Deionized water spray rinse and spin dry

f. Place wafer immediately in evaporator

39. Evaporate gold

a. Evaporate Au onto back side of wafer

b. Determine thickness by weighing test wafer

40. Alloy gold

    a. Anneal wafer for 3 minutes at 330°C in dry N_2

41. Electrical test

    a. Electrically test at probe station to determine breakdown voltage

42. Scribe apart

    a. Scribe wafers with diamond stylus at scribe station

    b. Separate individual devices with roller at scribe station

APPENDIX II

PHOTODIODE FABRICATION PROCESS MASKS

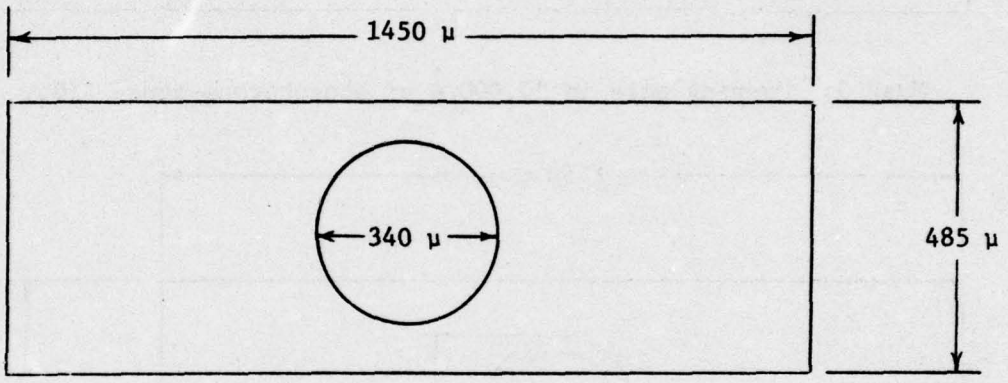

Mask 1: Opening hole in 4000 Å of SiO_2.

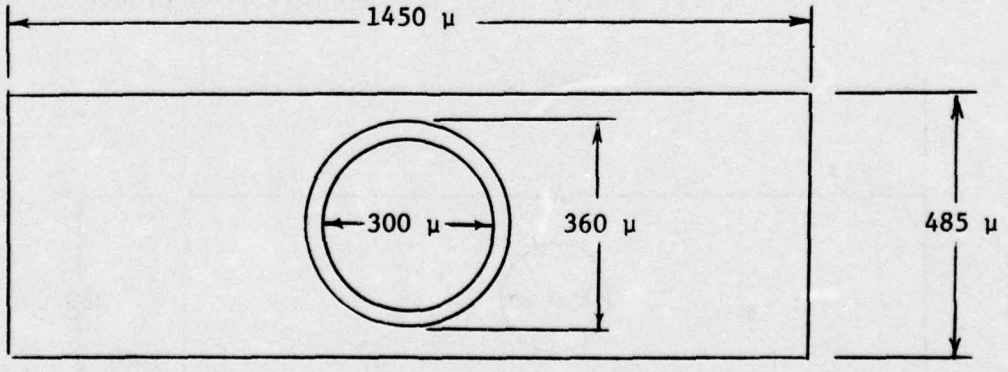

Mask 2: Initial mask for etching Si_3N_4.

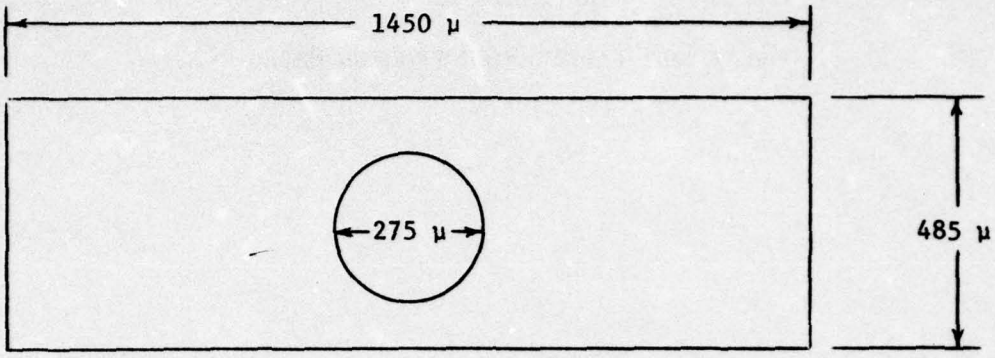

Mask 3: Opening hole in 20,000 Å of phosphorous-doped SiO_2.

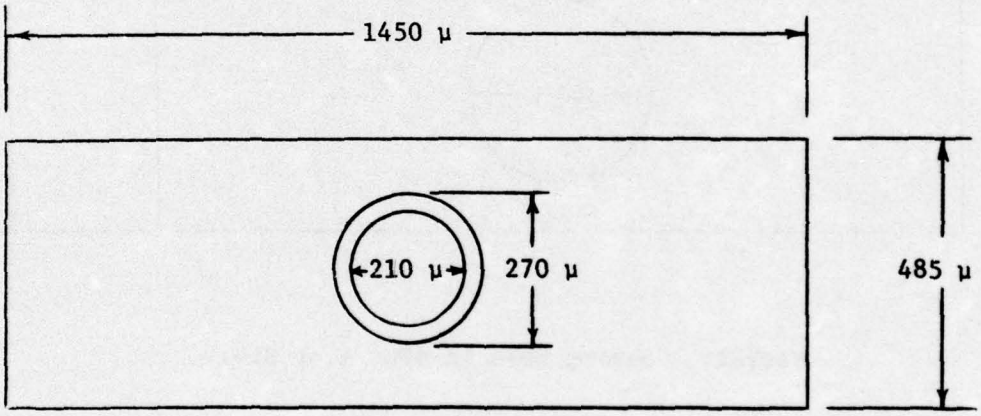

Mask 4: Opening hole in 1100 Å SiO_2 antireflection coating for making electrical contact to photodiode.

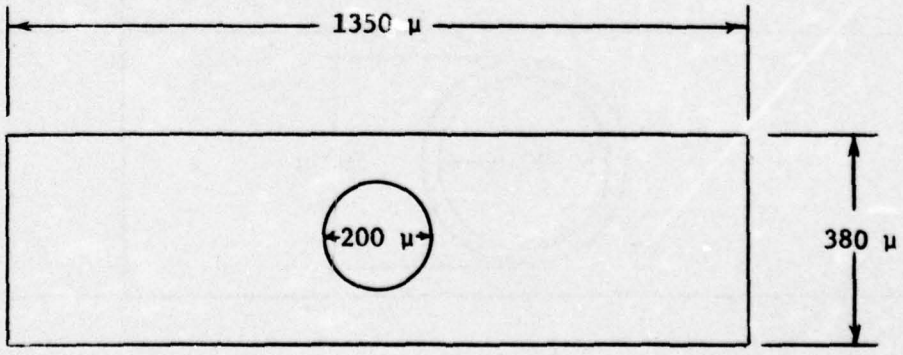

Mask 5: Aluminum mask to remove unwanted aluminum.

APPENDIX III

PREPARATION OF ETCHES AND STRIPPERS

The following is the make-up of the various etches and strippers that were used.

Aluminum Etch

200 ml deionized water (H_2O)

1600 ml phosphoric acid (H_3PO_4)

100 ml mitric acid (HNO_3)

100 ml acetic acid (CH_3COOH)

Use a glas graduate. Mix and store in an empty phosphoric acid bottle. Carefully shake the bottle (with the lid securely on) to mix the acids.

Oxide Etch

600 ml deionized water (H_2O)

440 ml hydrofluoric acid (HF)

2000 ml ammonium fluoride (NH_4F)

Use a plastic graduate. Mix and store in an empty ammonium fluoride bottle.

Boron Glass Etch

3000 ml deionized water (H_2O)

150 ml nitric acid (HNO_3)

100 ml hydrofluoric acid (HF)

Use a plastic graduate. Mix and store in an empty hydrofluoric acid bottle.

10:1 HF

3000 ml deionized water (H_2O)

300 ml hydrofluoric acid (HF)

Use a plastic graduate. Mix and store in an empty hydrofluoric acid bottle.

Chromic Acid

1 bottle (approximately 2210 ml)

sulfuric acid (H_2SO_4)

Heat to 90°C and then add:

100 gm chromium trioxide (Cr_2O_3)

Overlay Etch

1500 ml oxide etch

300 ml acetic acid (CH_3COOH)

Silicon Etch

1000 ml acetic acid (CH_3COOH)

1000 ml nitric acid (HNO_3)

50 ml hydrofluoric acid (HF)

Mix in an empty hydrofluoric acid bottle.

APPENDIX IV

MIXING PROCESS

The photodiode was designed for use at 6328 Å and designed to detect frequencies from dc through a cutoff frequency of greater than 11 GHz. In order to test this bandwidth criteria, a modulatable laser source was required. This paper describes the testing of the photodiode and how a free-running inhomogeneously broadened laser was used as a source of modulated light to obtain the frequency response of the photodiode.

Basically, the idea is to observe the beat frequencies[22] between the various longitudinal modes of an inhomogeneously broadened laser line. Figure A.1 represents the laser output as it might be observed

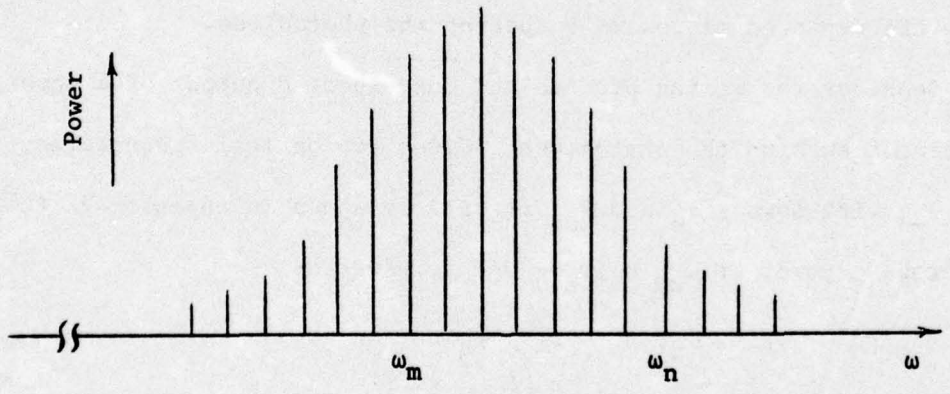

Fig. A.1. Possible laser output as seen through a scanning interferometer.

---

[22] W. R. Bennett, Jr., *Physical Review*, Vol. 126, April 15, 1962, pp. 580-593.

through a scanning interferometer. As a first approximation, the laser will operate in several longitudinal modes at frequencies ω_n with a frequency spacing between adjacent modes of $\delta = c/2L$, where c is the velocity of light and L is the length of the laser cavity. Beat frequencies between any of the modes can be observed with an appropriate square law detector. To first order, $\omega_n = 2\pi n\delta$, where n is a large integer on the order of 10^6; then the beat frequency between two modes n and m will be $\omega_{nm} = 2\pi\ |n - m|\delta$. In the laser used, the maximum ω_{nm} corresponds to a frequency on the order of 10.5 GHz.

The above is a very simple model of a real laser. In the first place, $\omega_n \neq 2\pi n\delta$ but is shifted from $2\pi n\delta$ due to "hole burning" and the general shape of the gain curve.[23] Another important point is that the mode amplitudes are coupled by the gain medium[24] and are not independent of one another. These effects must be kept in mind when predicting the expected microwave output of the photodiode.

Consider the mixing process and the expected output of a square law detector such as the photodiode. Given two optical frequencies, ω_n and ω_m, with powers P_n and P_m, it will be shown in Appendix VI that the microwave power at $\omega_{nm} = |\omega_n - \omega_m|$ is given by:

$$P_{\omega_{nm}} = 2R\left(\frac{en}{\hbar\omega}\right)^2 P_n P_m \qquad (A.1)$$

---

[23] *Ibid.*

[24] W. E. Lamb, Jr., *Physical Review*, Vol. 134, June 15, 1964, pp. A1429-A1450.

Here η is the quantum efficiency, $h\omega$ is the optical photon energy, e is the electron charge, and R represents the load impedance. For now, let

$$K = 2R\left(\frac{e\eta}{\hbar\omega}\right)^2 \tag{A.2}$$

In the laser, the P_n's are slowly varying functions of time compared with $e^{i\omega_n t}$; therefore Eq. A.1 can be written:

$$P\left(t, \omega_{nm}\right) = K\, P_n(t)\, P_m(t) \tag{A.3}$$

Now note that there is no way of keeping track of the individual mode powers, $P_n(t)$. The same holds true for $P\left(t, \omega_{nm}\right)$. The best that can be done is to find an average value for them. Define the following averages:

$$\overline{P_n(t)} = \frac{1}{2t_o}\int_{t-t_o}^{t+t_o} P_n(t)\, dt \tag{A.4}$$

$$\overline{P\left(t, \omega_{nm}\right)} = \frac{1}{2t_o}\int_{t-t_o}^{t+t_o} K\, P_n(t)\, P_m(t)\, dt \tag{A.5}$$

It is assumed $t_o >> 2\pi/\omega_{nm}$. Probability theory states that if $P_n(t)$ and $P_m(t)$ are independent variables, then Eq. A.5 reduces to:

$$\overline{P\left(t, \omega_{nm}\right)} = K\, \overline{P_n(t)}\, \overline{P_m(t)} \qquad (A.6)$$

It will be shown that the $\overline{P_n}$'s can be obtained from a measurement; however, as will become clear later, factors like $\overline{P\left(t, \omega_{nm}\right)}$ cannot be measured directly so that when Eq. A.6 is not true, there will be an error in using Eq. A.6 to estimate $\overline{P\left(t, \omega_{nm}\right)}$. This will tend to be a problem and will be considered in Appendix VIII.

Besides the problem associated with predicting the laser output, the diode in its circuit must be considered. The system that is actually under test is the photodiode mounted on the end of a tapered transmission line plus a dc-biasing T.[25] This is shown in Fig. A.2.

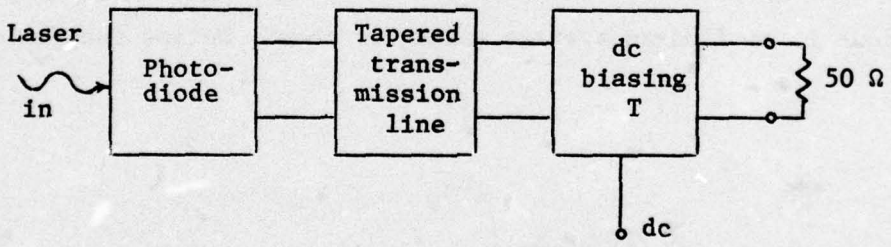

Fig. A.2. Photodiode circuit.

In Appendix V, a model for the photodiode as actually tested is developed which can be used to predict the output given the input signal. In Appendix VI, the mixing of the laser modes is discussed and

---

[25] C. K. Petersen, *op. cit.*

two possible ways of measuring the power are developed. Appendix VII is devoted to a discussion of the laser and the effects of mode coupling. Appendix VII also describes the actual laser output and develops a model for that output. Appendix VIII describes the actual output of a spectrum analyzer and the effects of frequency shift from $f_{nn} = |n - m|\delta$ are bought into the model. Appendix IX describes the experimental procedure and gives the experimental results. Appendix X describes the predicted results and compares them with the experiment.

APPENDIX V

EQUIVALENT CIRCUIT FOR PHOTODIODE

An equivalent circuit for the photodiode and its circuit is needed in order to predict the expected output as a function of frequency. Figure A.3 shows approximately how the diode is mounted on the

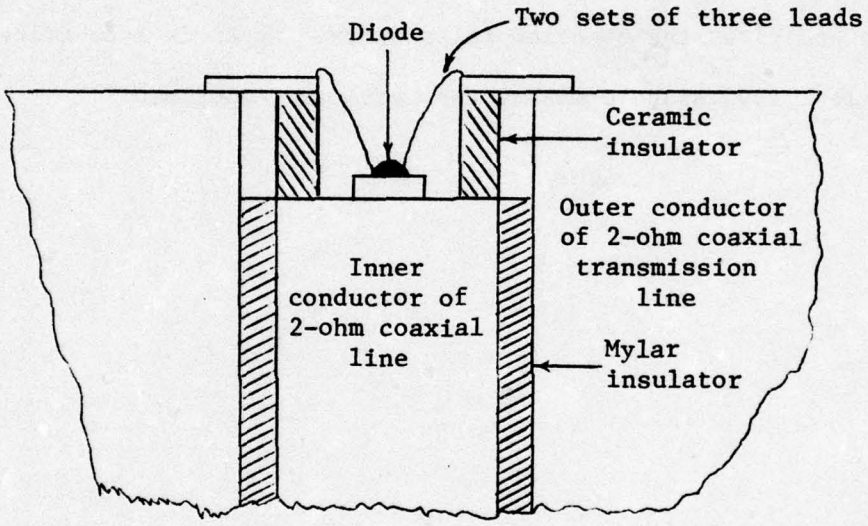

Fig. A.3. Diode as mounted on the end of the taper.

end of the tapered transmission line. Clearly, the transmission line suffers a large discontinuity as the center conductor is terminated. After the diode is encountered, the two sets of three leads together with the outer conductor and insulator will constitute a short section of transmission line of length ℓ. The properties of this line are difficult to estimate accurately since it is a nonuniform line. An equivalent circuit is shown in in Fig. A.4. The diode is represented

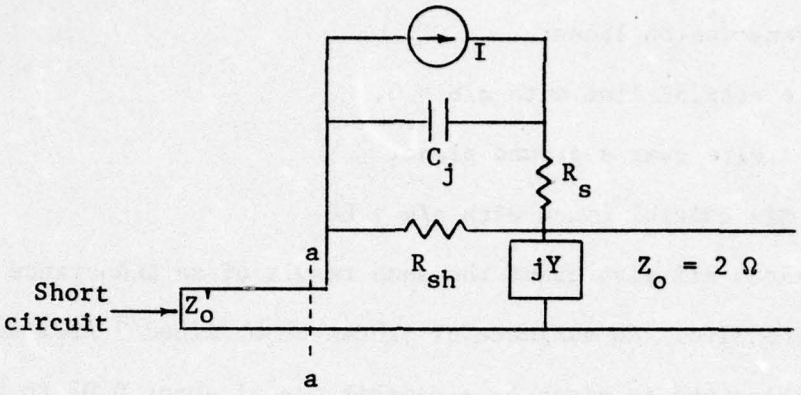

Fig. A.4. Equivalent circuit of diode and transmission line.

by a current generator, I (assumed to vary as $e^{i\omega t}$), a junction capacitance C_j, and a series R_s and a shunt R_{sh} resistance. The lead wires are represented by a transmission line with characteristic impedance Z_o'. The discontinuity at the end of the 2-ohm line is represented by an admittance jY.

Projecting the short in the Z_o' line back to a-a, the impedance found at a-a is

$$X = j\, Z_o' \tan \beta\ell$$

For frequencies from 2 to 10 GHz, $0.04 \leq \beta\ell \leq 0.2$ and $\tan \beta\ell \simeq \beta\ell$, hence

$$X = j\, \frac{Z_o'\ell}{c}$$

i.e., it appears that there is an inductor at a-a with an inductance

$L = Z_o' \ell / c$. An estimate for L can be obtained by looking at various forms of transmission lines:

1. A coaxial line with $a/b \simeq 3$.
2. A wire over a ground plane.
3. Six coaxial lines with $a/b \simeq 60$.

These estimates all give about the same result of an inductance of 0.4 to 0.8 nanohenries. An estimate of jY can be obtained[26] from curves of discontinuities and is given by a capacitance of about 0.02 to 0.1 pF. With this in mind, the circuit of Fig. A.4 reduces to Fig. A.5.

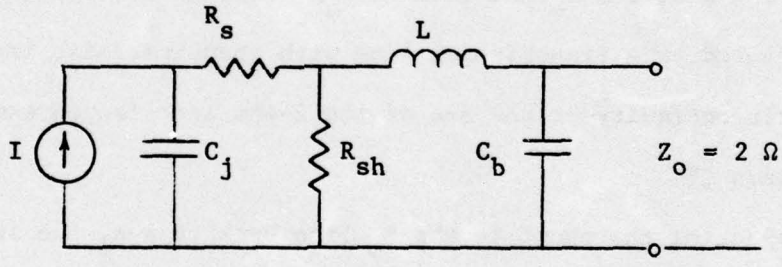

Fig. A.5. Diode to taper equivalent circuit.

This circuit can be transformed to Fig. A.6, and two ports 1 and 2 can be defined. Using two-port network theory, it can be shown that

---

[26] *Microwave Engineer's Handbook*, Artech House, Inc., Dedham, Massachusetts, Vol. 1, 1971, p. 111.

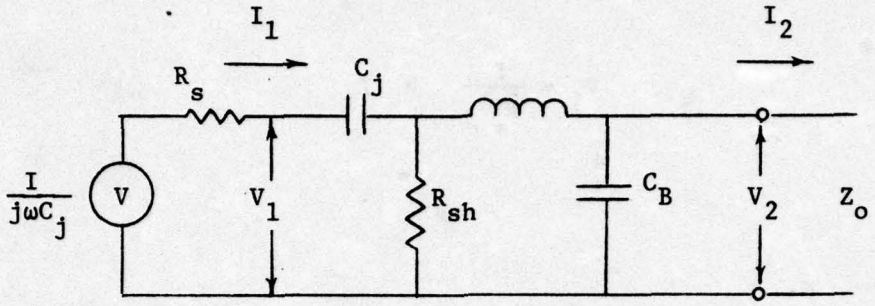

Fig. A.6. Transformed network.

$$\begin{bmatrix} V_2 \\ -I_2 \end{bmatrix} = \begin{bmatrix} B & -A \\ -\frac{1}{A}(BC - 1) & C \end{bmatrix} \begin{bmatrix} V_1 \\ I_1 \end{bmatrix} \tag{A.7}$$

where

$$A = \frac{L}{C_j R_{sh}} + j\left(\omega L - \frac{1}{\omega C_j}\right) \tag{A.8a}$$

$$B = 1 + \frac{j\omega L}{R_{sh}} \tag{A.8b}$$

$$C = 1 - \omega^2 L C_B + \frac{C_B}{C_j} + j\left(\frac{L}{R_{sh}} \cdot \frac{C_B}{C_j} - \frac{1}{\omega C_j R_{sh}}\right) \tag{A.8c}$$

The input voltage V_1 is given by:

$$V_1 = \frac{I}{j\omega C_j} - R_s I_1$$

or

$$\frac{I}{j\omega C_j} = V_1 + R_s I_1$$

Multiply through by $1/\sqrt{8R_s}$ to obtain

$$\frac{I}{j\omega C_j\sqrt{8R_s}} = \frac{1}{\sqrt{iR_s}}\left(V_1 + R_s I_1\right) \qquad \text{(A.9)}$$

The right-hand side of Eq. A.9 looks very much like the normal-mode solution[27] of transmission line of characteristic impedance R_s. If the definition

$$a_1^+ = \frac{I}{j\omega C_j\sqrt{8R_s}} \qquad \text{(A.10)}$$

is made, then Fig. A.6 transforms to Fig. A.7.

This is the most convenient circuit to work with. $a_1^+ a_1^{+*}$ is the time average power entering port 1 and is the power out of the diode due to the laser. $a_2^+ a_2^{+*}$ is the time average power entering port 2 and

---

[27] C. C. Johnson, *Field and Wave Electrodynamics*, McGraw-Hill Book Company, Inc., New York, 1965, pp. 124-126.

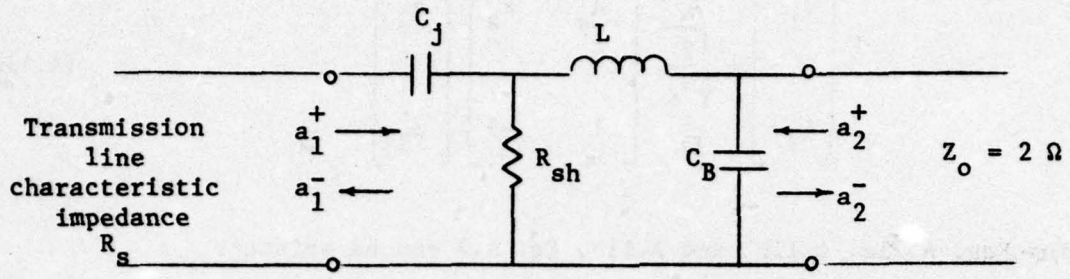

Fig. A.7. Transmission line equivalent circuit.

is the reflected power from the taper, biasing-T, and load circuit. $a_2^- a_2^{-*}$ is the time average power leaving port 2. $a_1^- a_1^{-*}$ is the reflected power from the total circuit to the right of port 1. It can either be assumed that the line R_s is infinitely long or is terminated in a generator of impedance R_s but, at any rate, the wave a_1^- will not be reflected back into port 1. The a's, V's, and I's are related by:

$$\begin{bmatrix} a_2^- \\ a_2^+ \end{bmatrix} = \frac{1}{\sqrt{8Z_o}} \begin{bmatrix} 1 & Z_o \\ 1 & -Z_o \end{bmatrix} \begin{bmatrix} V_2 \\ -I_2 \end{bmatrix} \tag{A.11a}$$

$$\begin{bmatrix} a_1^+ \\ a_1^- \end{bmatrix} = \frac{1}{\sqrt{8R_s}} \begin{bmatrix} 1 & R_s \\ 1 & -R_s \end{bmatrix} \begin{bmatrix} V_1 \\ I_1 \end{bmatrix} \tag{A.11b}$$

$$\begin{bmatrix} V_1 \\ \\ I_1 \end{bmatrix} = \sqrt{\frac{2}{R_s}} \begin{bmatrix} R_s & R_s \\ \\ 1 & -1 \end{bmatrix} \begin{bmatrix} a_1^+ \\ \\ a_1^- \end{bmatrix} \tag{A.11c}$$

Using Eqs. A.11a, A.11b, and A.11c, Eq. A.7 can be written:

$$\begin{bmatrix} a_2^- \\ \\ a_2^+ \end{bmatrix} = \frac{1}{\sqrt{4R_s Z_o}} \begin{bmatrix} 1 & Z_o \\ \\ 1 & -Z_o \end{bmatrix} \begin{bmatrix} B & -A \\ \\ -\frac{1}{A}(BC - 1) & C \end{bmatrix} \begin{bmatrix} R_s & R_s & a_1^+ \\ \\ 1 & -1 & a_1^- \end{bmatrix} \tag{A.12}$$

Performing the matrix multiplication, the following relation is obtained:

$$\begin{bmatrix} a_2^- \\ \\ a_2^+ \end{bmatrix} = \begin{bmatrix} T_{11} & T_{12} \\ \\ T_{21} & T_{22} \end{bmatrix} \begin{bmatrix} a_1^+ \\ \\ a_1^- \end{bmatrix} \tag{A.13}$$

where

$$T_{11} = \frac{1}{2} \frac{1}{Z_o R_s} \left\{ R_s B - A - Z_o R_s \cdot \frac{1}{A}(BC - 1) + Z_o C \right\} \tag{A.14a}$$

$$T_{12} = \frac{1}{2} \frac{1}{Z_o R_s} \left\{ R_s B + A - Z_o R_s \cdot \frac{1}{A}(BC - A) - Z_o C \right\} \tag{A.14b}$$

$$T_{21} = \frac{1}{2} \frac{1}{Z_o R_s} \left\{ R_s B - A + Z_o R_s \cdot \frac{1}{2}(BC - A) - Z_o C \right\} \tag{A.14c}$$

$$T_{22} = \frac{1}{2} \frac{1}{Z_o R_s} \left\{ R_s B + A + Z_o R_s \cdot \frac{1}{2}(BC - A) + Z_o C \right\} \tag{A.14d}$$

The matrix in Eq. A.13 is known as a T-matrix.[28] It can be derived from the scattering matrix of the network and is useful since it can be cascaded with the other T-matrices of the system. Since the network is reciprocal, the T_{ij}'s are related by

$$T_{11}T_{22} - T_{21}T_{22} = 1 \tag{A.15}$$

The reflection coefficient at port 2 is defined as

$$r = \frac{a_2^+}{a_2^-} \quad \text{or} \quad a_2^+ = ra_2^- \tag{A.16}$$

Using Eqs. A.16 and A.13 along with Eq. A.15, it is found that

$$a_2^- = \frac{1}{T_{22} - T_{12}\,r}\, a_1^+ \tag{A.17}$$

If the circuit from the taper on is a good match, then $r \simeq 0$ and

$$a_2^- a_2^{-*} \simeq \frac{1}{|T_{22}|^2}\, a_1^+ a_1^{+*}$$

$a_2^- a_2^{-*}$ is the expected time average output power, and $a_1^+ a_1^{+*} = |I|^2/8\omega^2 C_j^2 R_s$, the input power, hence the time average expected output power, $\bar{P}_o$, is (note that $|I|^2$ is a time average):

---

[28] S. Ramo, J. R. Whinnery, and T. VanDuzer, *Fields and Waves in Communications Electronics*, John Wiley and Sons, New York, 1967, pp. 609-611.

$$\overline{P}_o = \frac{1}{8\omega^2 C_j^2 R_s \left|T_{22}\right|^2} \left|I\right|^2 \qquad \text{(A.18)}$$

If a good match does not exist, then $\overline{P}_o$ will be different. It is expected, however, that the taper and biasing-T will present a low VSWR, and hence small r. All that is needed now is to find $\left|I\right|^2$ in order to predict the output.

APPENDIX VI

DERIVATION OF DIODE CIRCUIT

Consider the detection of light by a photodiode. A photon striking the surface will have a probability of ionizing an electron into the conduction band, causing current to flow. This current will be

$$i = \eta ne \tag{A.19}$$

Here, η is the quantum efficiency in number of electrons excited to the conduction band per photon, n is the number of photons, and e is the electric charge. The total power in the beam is

$$P_T = nhf \tag{A.20}$$

Hence Eq. A.20 can be written

$$i = \left(\frac{ne}{hf}\right) P_T \tag{A.21}$$

Now the total power in the field is

$$P_T = KEE^* \tag{A.22}$$

where K is a constant. The field of the laser can be written as

$$E = \sum_{\ell=-M/2}^{M/2} E_\ell(t)\, e^{j\left(\omega_\ell t+\phi_\ell\right)} \tag{A.23}$$

Here, M is the number of longitudinal modes (assumed odd; see Fig. 8) for labeling scheme: ω_o is the center frequency of the laser line, and the numbering system starts there; as an example, $\omega_{-6} \simeq \omega_o - 6 \cdot (2\pi\delta)$ and $\omega_6 \simeq o_o + 6(2\pi\delta)$), and the mode field amplitudes $E_\ell(t)$ are slowly varying real functions of time as are the ω_ℓ's and ϕ_ℓ's (this point will be shown later). Using Eq. A.22 becomes

$$P_T = \sum_{\ell=-M/2}^{M/2} KE_\ell^2(t) + \sum_{\ell=-M/2}^{M/2} \sum_{m>\ell}^{M/2} 2KE_\ell(t)\, E_m(t)\, \cos\left(\left(\omega_\ell - \omega_m\right)t + \phi_\ell - \phi_m\right) \tag{A.24}$$

Identifying $P_\ell(t) = KE_\ell^2(t)$, Eq. A.24 becomes

$$P_T = \sum_{\ell=-M/2}^{M/2} P_\ell(t) + \sum_{\ell=-M/2}^{M/2} \sum_{m>\ell}^{M/2} 2\sqrt{P_\ell(t)P_m(t)}\, \cos\left\{\left(\omega_\ell - \omega_m\right)t + \phi_\ell - \phi_m\right\} \tag{A.25}$$

It has been observed that laser power measured with a detector of a bandwidth ≈20 kHz is constant. This power is given by the first term in Eq. A.25. Combining Eqs. A.21 and A.25, remembering that it has been observed that $\sum P_\ell(t)$ is a constant,

$$i(t) = i_o + \frac{2\eta e}{hf} \sum_{\ell=-M/2}^{M/2} \sum_{m>\ell}^{M/2} \sqrt{P_\ell(t)P_m(t)} \cos \left\{ (\omega_\ell - \omega_m)t + \phi_\ell - \phi_m \right\} \tag{A.26}$$

In any experimental procedure, the dc current can be blocked so that only the RF portion can be observed. Define

$$i_{RF} = \frac{2\eta e}{hf} \sum_{\ell=-M/2}^{M/2} \sum_{m>\ell}^{M/2} \sqrt{P_\ell(t)P_m(t)} \cos \left\{ (\omega_\ell - \omega_m)t + \phi_\ell - \phi_m \right\} \tag{A.27}$$

From Eq. A.27, it is seen i_{RF} contains 1/2 M(M - 1) different signals; however, by referring to Fig. A.8, it is seen that M - 1 of the signal

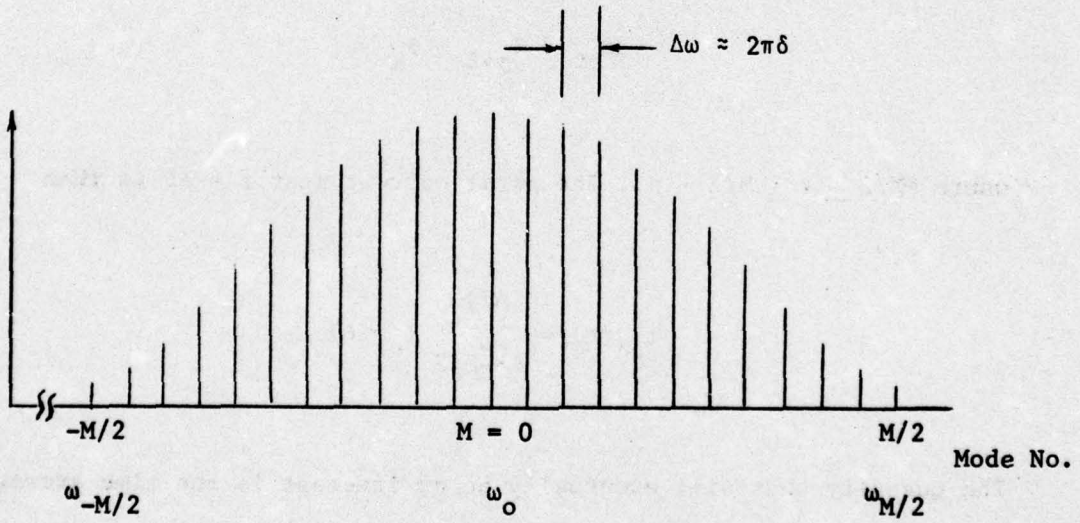

Fig. A.8. Representation of laser mode structure.

have a beat frequency close to δ, M - 2 have a frequency close to 2δ, and in general M - 1 - m close to $m\delta$, m an integer, and $m < M - 1$. It will be seen later that the M - 1 - m signal with a frequency close to $m\delta$ are all grouped within a 500 kHz interval of one another. Hence, a conventional microwave spectrum analyzer can be used to separate the frequency close to the various $m\delta$'s and the structure can be observed.

Let ρ be an integer and indicate the difference in the mode number so that $\rho\delta$ is the approximate beat frequency. Define

$$i_{\rho\ell}(t) = \frac{2e\eta}{h\omega} \sqrt{P_\ell(t)P_{\ell+\rho}(t)} \cos\left(\omega_{\rho\ell}t + \phi_{m\ell}\right) \tag{A.28}$$

$$\omega_{\rho\ell} = \omega_{\rho+\ell} - \omega_\ell \quad (\simeq 2\pi\rho\delta) \tag{A.29a}$$

$$\phi_{\rho\ell} = \phi_{\rho+\ell} - \phi_\ell \tag{A.29b}$$

where $-M/2 \leq \ell \leq M/2 - \rho$. The total current near $f = \rho\delta$ is then

$$i_{\rho\delta}(t) = \sum_{\ell=-M/2}^{M/2-\rho} i_{\rho\ell}(t) \tag{A.30}$$

The quantity that will eventually be of interest is the time average of $i^2_{\rho\delta}(t)$. This can most easily be done by squaring Eq. A.30 and ignoring terms that oscillate at $\omega = 2(2\pi\rho\delta)$. The result is

$$\overline{i^2_{\rho\delta}(t)} = 2\left(\frac{\eta e}{hf}\right)^2 \sum_{\ell=-M/2}^{M/2-\rho} \left\{ P_\ell(t)P_{\rho+\ell}(t) \right.$$

$$\left. + 2 \sum_{k>\ell}^{M/2-\rho} \sqrt{P_\ell(t)P_{\ell+\rho}P_k(t)P_{k+\ell}(t)} \cos\left[(\omega_{\rho\ell} - \omega_{\rho k})t + \phi_{\rho\ell} - \phi_{\rho k}\right] \right\}$$

(A.31)

Consider the information contained in Eq. A.31. Equation A.31 together with Eq. A.18 represent the expected power output of a band pass filter centered at $\omega = 2\rho o\delta$ and the photodiode and a method for obtaining a frequency response for the photodiode. Equation A.31 will be returned to later and the possible error involved will be discussed.

A microwave spectrum analyzer might also be used as a measuring system. Equation A.28 can be written

$$i_{\rho\omega}(t) = \frac{2\eta e}{hf} \sqrt{P_\ell(t)P_{\ell+\rho}(t)} \left\{ \cos \omega_{\rho\ell} t \cos \phi_{\rho\ell} - \sin \omega_{\rho\ell} t \sin \phi_{\rho\ell} \right\}$$

Defining $f_{\rho\ell}(t) = \sqrt{P_\ell(t)P_{\ell+\rho}(t)}$ and letting $I_{\rho\ell}(\omega)$ and $F_{\rho\ell}(\omega)$ be the Fourier transforms of $i_{\rho\ell}(t)$ and $f_{\rho\ell}(t)$, respectively, then

$$I_{\rho\ell}(\omega) = \frac{e\eta}{hf} \left\{ e^{j\phi_{\rho\ell}} F_{\rho\ell}(\omega - \omega_{\rho\ell}) + e^{-j\phi_{\rho\ell}} F_{\rho\ell}(\omega + \omega_{\rho\ell}) \right\} \qquad \text{(A.32)}$$

To a first approximation,

$$F_{\rho\ell}(\omega \pm \omega_{\rho\ell}) \simeq \sqrt{P_\ell(t)P_{\ell+\rho}(t)}\ \delta(\omega \pm \omega_{\rho\ell})$$

Here the fact that the $P_\ell(t)$'s are slowing varying functions of time has been used. With this assumption, $I_{\rho\ell}(\omega)$ becomes

$$I_{\rho\ell}(\omega) = \frac{e\eta}{hf}\sqrt{P_\ell(t)P_{\ell+\rho}(t)}\left\{e^{j\phi_{\rho\ell}}\ \delta(\omega - \omega_{\rho\ell}) + e^{j\phi_{\rho\ell}}\ \delta(\omega + \omega_{\rho\ell})\right\} \quad (A.33)$$

and forming the sum of all the terms near $\rho\delta$,

$$I_{\rho\delta}(\omega) = \frac{e\eta}{hf}\sum_{\ell=-M/2}^{M/2-\rho}\sqrt{P_\ell(t)P_{\ell+\rho}(t)}\left\{e^{j\phi_{\rho\ell}}\ \delta(\omega - \omega_{\rho\ell}) + e^{-j\phi_{\rho\ell}}\ \delta(\omega + \omega_{\rho\ell})\right\} \quad (A.34)$$

What will be displayed on the spectrum analyzer face will be proportional to either $|I_{\rho\delta}(\omega)|$, $|I_{\rho\delta}(\omega)|^2$, or $\log_{10}|I_{\rho\delta}(\omega)|$. Using Eq. A.34 and remembering that $\delta(\omega_{\rho\ell} + \omega_{\rho k}) \equiv 0$ for all ℓ and k, it is found that

$$I_{\rho\delta}(\omega)^2 = \left(\frac{e\eta}{hf}\right)^2 \sum_{\ell=-M/2}^{M/2-\rho}\left[\delta(\omega - \omega_{\rho\ell}) + \delta(\omega - \omega_{\rho\ell})\right]\left\{P_\ell(t)P_{\ell+\rho}(t)\right.$$

$$+ 2\sum_{k>\ell}^{M/2-\rho}\sqrt{P_\ell(t)P_{\ell+\rho}(t)P_k(t)P_{k+\rho}(t)}$$

$$\left.\cdot\ \cos\left(\phi_{\rho\ell} - \phi_{\rho k}\right)\delta(\omega_{\rho\ell} - \omega_{\rho k})\right\} \quad (A.35)$$

Equation A.35 contains the essence of what will be displayed by a spectrum analyzer. Of course only the $\delta(\omega - \omega_{\rho\ell})$ term will be displayed; however, it can be seen that the overall shape will depend on the density of the various $\omega_{\rho\ell}$'s. It might be thought at first that the $\delta(\omega_{\rho\ell} \text{ p } \omega_{\rho k})$ will always be zero; however, this may not be the case, as will be seen later. Also, the δ-functions should not be taken too literally. It was assumed that $F_{\rho\ell}(\omega - \omega_{\rho\ell}) = \sqrt{P_{\ell}(t)P_{\ell+\rho}(t)}\ \delta(\omega - \omega_{\rho\ell})$; however, this is only an approximation. $F_{\rho\ell}(\omega - \omega_{\rho\ell})$ will have a bandwidth of a few kilohertz. This presents no problems as long as the receiver width on the spectrum analyzer is a few kilohertz. In order to interpret Eqs. A.31 or A.35, a clearer understanding of the laser's operation is needed. To this end, an understanding of mode coupling effects and the frequency distribution of the mixed frequencies is needed. The only laser available with a line width of about 11 GHz was an argon ion laser tuned to the 5145 Å line, hence all further discussion is referenced to it.

APPENDIX VII

MODE COUPLING EFFECTS

To understand the effects of mode coupling on the expected diode output, it is necessary to obtain at least a good qualitative understanding of the laser characteristics.

The argon laser, like many gas lasers, has a doppler broadened gain curve due to the thermal velocities of the atom in the gain medium.[29] Since the atomic line width of the laser transition is usually narrow compared to the doppler broadened line width, a traveling wave of frequency f will only interact with atoms whose velocity u is close to $u = c(f - f_o)/f_o$, where f_o is the center frequency of the transition. Such a wave will "burn a hole" in the gain curve of the medium due to the depopulation of the upper laser level. This is illustrated in Fig. A.9.

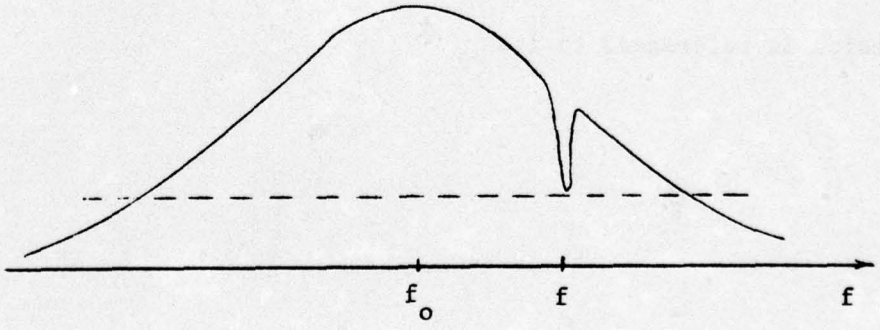

Fig. A.9. Hole burning due to a traveling wave.

---

[29] For a good review of doppler broadening and its effects, see A. E. Siegman, *An Introduction to Lasers and Masers*, McGraw-Hill Book Company, Inc., New York, 1971, Chapter 9.

In most lasers, standing waves rather than traveling waves exist. This leads to double hole burning by a single frequency. This can be seen by breaking the standing wave into two traveling waves. The forward wave will interact with atoms at a velocity $u = c(f - f_o)/f_o$, and the backward wave with atoms at $u = -c(f - f_o)/f_o$. That is, a wave at f burns two holes in the gain curve, one at f and one at $2f_o - f$, as shown in Fig. A.10.

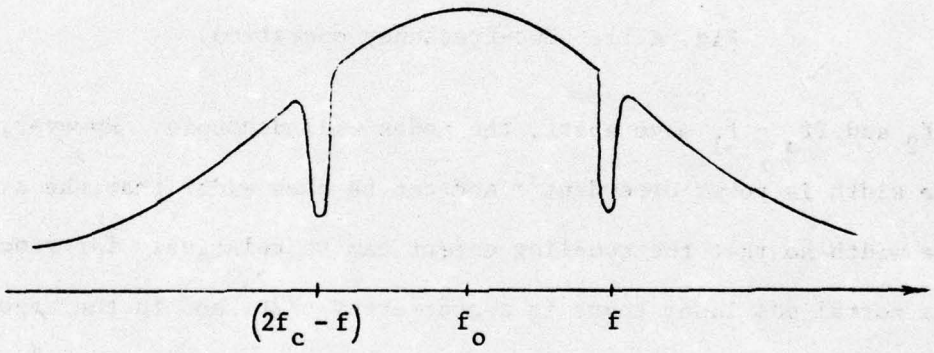

Fig. A.10. Double hole burning.

Now consider the possibility of oscillation at two modes at frequencies f_1 and f_2. Each mode will burn two holes in the gain curve as shown in Fig. A.11.

As f_2 approaches $2f_o - f_1$ $(f_1 \to 2f_o - f_2)$, the two modes will be using the same atoms of the gain medium; i.e., the two modes will be competing with each other. This situation tends to be unstable near threshold. Clearly, the two laser modes are coupled by the gain medium.

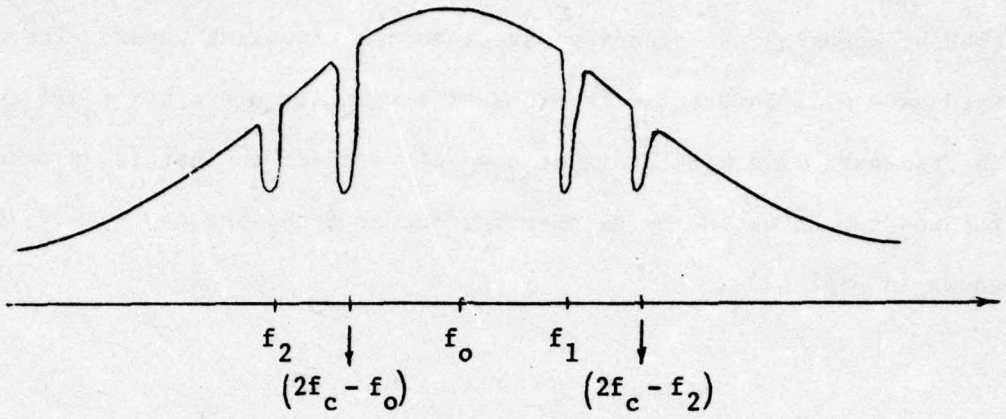

Fig. A.11. Two-frequency operation.

As f_2 and $2f_o - f_1$ move apart, the modes will decouple. However, the hole width is power dependent[30] and can be much wider than the atomic line width so that the coupling effect can be relatively far reaching. In a normal gas laser there is a mode every c/2L, and in the argon laser the minimum hole width will be on the order of 0.108 GHz ~ c/2L for the laser to be used, which implies mode coupling cannot be avoided.

The effect of the holes along with the general slope of the gain curv.. also effect the operating frequency of each mode. This is a result of the fact that the real and imaginary parts of the susceptibility are related by the Kramer-Kronig relation[31] (they are Hilbert transforms of one another). The imaginary part of the susceptibility is

---

[30] W. R. Bennett, Jr., *op. cit.*

[31] R. H. Pantell and H. E. Puthoff, *Fundamentals of Quantum Electronics*, John Wiley and Sons, Inc., New York, 1969, p. 70.

directly proportional to the shape of the gain curve and shows the effects of the holes. The real part of the susceptibility goes into the determination of the mode frequencies and hence the effect of the holes on the operating frequency.[32]

What should be seen from the discussion of Chapter IV is the fields of the laser modes interact with each other through the gain medium. Both the amplitude and frequency of a mode are affected by neighboring modes as well as by modes on the opposite side of the gain curve so that the amplitudes and frequencies of the various modes are not independent. All the theories[33] that describe multimode operation are based on a perturbation expansion of the density matrix whose terms go like $(\mu E/\hbar)^n$, where μ is the dipole matrix element for the transition and E is the electric field strength. An estimation of $\mu E/h$ shows it to be on the order of 10^3-10^5 for the laser being used; i.e., the expansion diverges. What is clear is the theories are good only near threshold where they work well. Threshold theories predict that modes on opposite sides of the gain curve will be mutually exclusive in the steady state. Direct observation of the laser to be used, using a scanning interferometer, indicates two modes on opposite sides of the gain curve are not mutually exclusive although they are surely not independent. Figure 12 shows a photo of a single sweep by the inteferometer.

---

[32] W. R. Bennett, Jr., *op cit.*

[33] For a review of these theories, see M. Sargent, III, M. O. Scully, and W. E. Lamb, Jr., *Laser Physics*, Addison-Wesley Publishing Company, Reading, Massachusetts, 1974, Chapters IX and X.

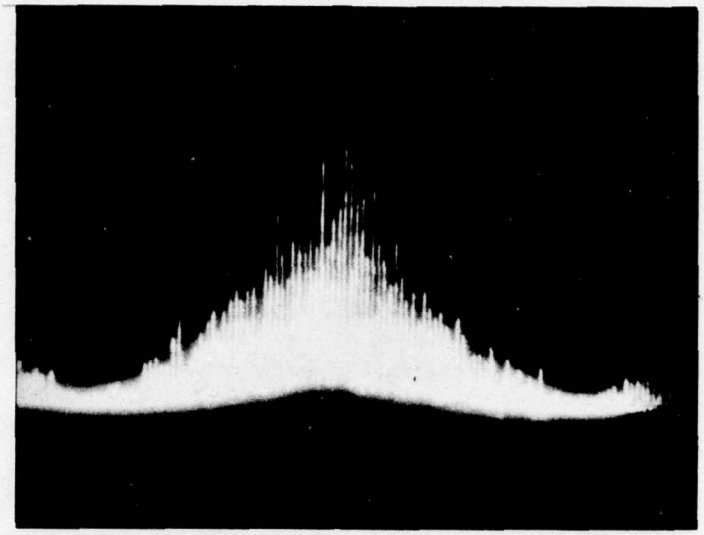

Fig. A.12. Single sweep exposure.

Over the long run, the modes seem to tend to a well defined average. Figure 13 shows a photo where approximately fifty sweeps of the

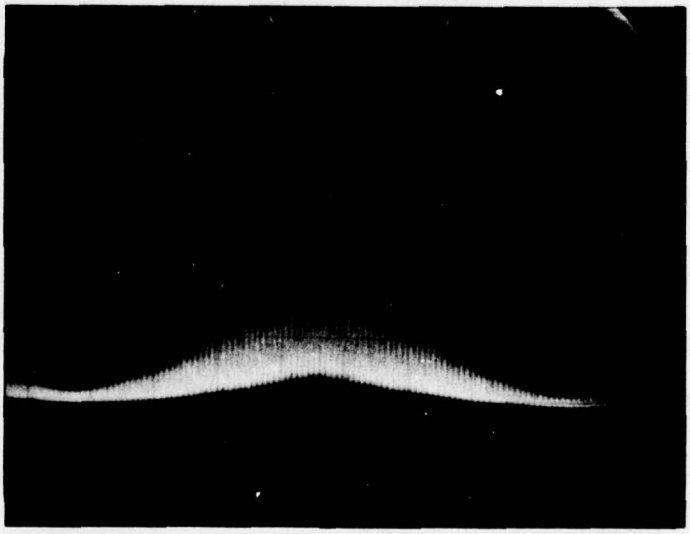

Fig. A.13. Multiple sweep exposure.

interferometer contributed to the exposure.

Because the laser modes appear to tend to some definite average value, a model will be developed based on the assumption that they do. It will be assumed that a spectrum analyzer will be used and Eq. A.35 will apply. Since averages are being considered, it will be assumed that the terms containing $\cos\left(\phi_{\rho\ell} - \phi_{\rho k}\right)$ will be zero.

In both Eqs. A.31 and A.35, $L_{\rho\delta}(t)$ or $|I_{\rho\delta}(\omega)|^2$ are proportional terms like $P_n P_{n+\rho}$. Assume now that P_n is given by

$$P_n = P_o\, e^{-\left[\left(\omega_o + 2\pi n\delta\right) - \omega_o\right]^2/2\sigma^2} = P_o\, e^{-(2\pi n\delta)^2/2\sigma^2} \qquad \text{(A.36)}$$

where $\sigma = \Delta\omega\left(2^3 \ln 2\right)^{-1/2}$, $\Delta\omega$ being the full width at half maximum of the laser output power spectrum. (The presumption is made that since the driving polarization has a Gaussian distribution about ω_o, so will the output power spectrum.) $\Delta\omega$ can be read off the photograph of the laser spectrum. The integer n will take on the values from -M/2 to +M/2 where M + 1 is the number of modes and M is assumed to be even for simplicity. Figure 14 shows this arrangement.

Let $\alpha = (2\pi\delta)^2/2\sigma^2$, then $P_n = P_o\, e^{-\alpha n^2}$. In the context of Eq. A.35, $|I|^2$ due to modes P_n and $P_{n+\rho}$ is

$$|I_{\rho\delta}|^2_{n,\, n+\rho} \propto P_o^2\, e^{-\alpha\left(n^2 + (n+\rho)^2\right)} \qquad \text{(A.37)}$$

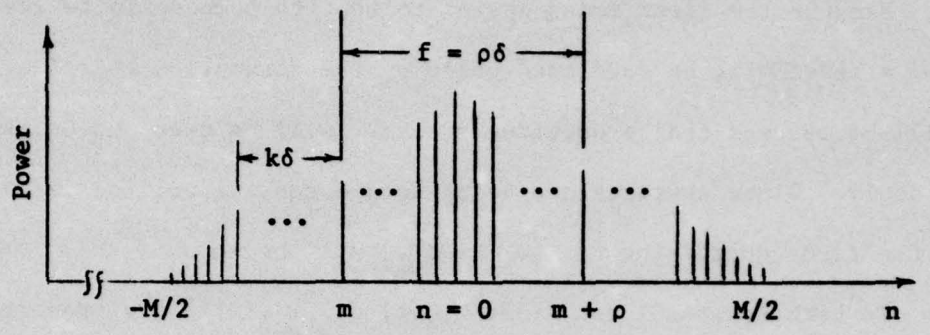

Fig. A.14. Laser mode structure used for calculation of expected $|I|^2$ for two modes.

For fixed ρ, $|I|^2_{n,\ n+\rho}$ will be a maximum when $n = -\rho/2$ for ρ even (for ρ odd, two sets of modes will have the same $|I|^2$ value, but the arguments and result will have the same meaning), and $|I_{\rho\delta}|^2_{n,\ n+\rho}$ is given by

$$|I_{\rho\delta}|^2_{-\frac{\rho}{2},\ \frac{\rho}{2}} \propto P_o^2\, e^{-\alpha\left(\rho^2/2\right)} \tag{A.38}$$

Now define $n = -\rho/2 + k$ where $-M/2 + \rho/2 \leq k \leq M/2 - \rho/2$ (k describes how far in frequency we are from the maximum position), and using Eq. A.37, the following result is obtained:

$$|I_{\rho\delta}|^2_{-\frac{\rho}{2}+k,\ \frac{\rho}{2}+k} \propto P_o^2 \exp\left[-\alpha\,\frac{\rho^2}{2}\right]\left[\exp\left(-4\alpha k^2\right)\right]$$

or

$$|I_{\rho\delta}|^2_{-\frac{\rho}{2}+k,\,\frac{\rho}{2}+k} = |I_{\rho\delta}|^2_{-\frac{\rho}{2},\,\frac{\rho}{2}} \cdot \exp\left(-4\alpha k^2\right) \qquad \text{(A.39)}$$

It appears that for the laser to be used, $\alpha \approx 0.0009$ to 0.0011.

APPENDIX VIII

THE DATA

A microwave spectrum analyzer was used to observe the mixed frequency output. What appeared on the spectrum analyzer screen is shown in Figs. A.15 through A.18, representing four different mixed frequencies. The total width of the lines is on the order of 500 kHz in each case. Clearly, the mixed frequencies for two different sets of laser modes do not fall directly on one another, which is as expected. Briefly consider the factors which determine the value of the mixed frequency.

The laser frequencies themselves are determined from the relation

$$\mathrm{Re}\left[\int_0^L k(z)\,dz\right] = n\pi \qquad n = 0, 1, \ldots \tag{A.40}$$

where $k(z)$ is the propagation constant for the nth mode. For the laser being used, n is on the order of 10^6. L is the length of the laser cavity. All that is required for now is a general feeling for the situation; hence it will be assumed that the gain medium fills the cavity and is constant throughout. This may not be a good assumption but will be used as a starting point. With these assumptions, Eq. A.40 reduces to

$$\mathrm{Re}\,[kL] = n\pi \tag{A.41}$$

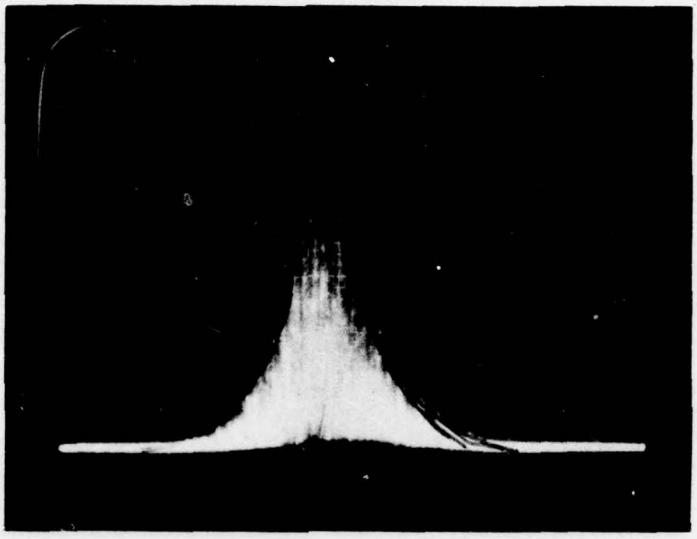

Fig. A.15. Microwave power spectrum near $\rho\delta$ = 2.725 GHz (100 kHz/div). Spectrum analyzer resolution: 5 kHz.

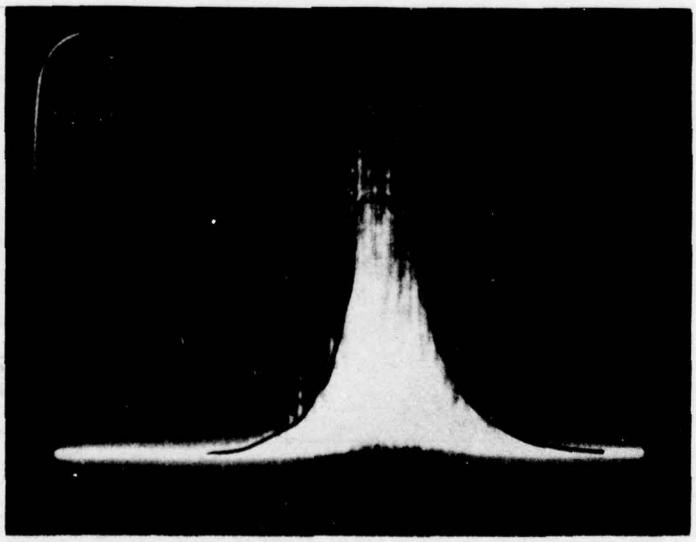

Fig. A.16. Microwave power spectrum near $\rho\delta$ = 3.99 GHz (100 kHz/div). Spectrum analyzer resolution: 5 kHz.

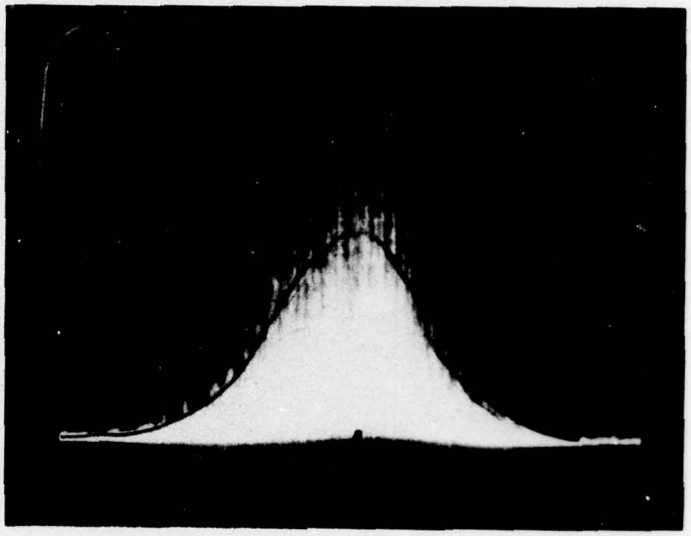

Fig. A.17. Microwave power spectrum near $\rho\delta$ = 7.16 GHz (100 kHz/div). Spectrum analyzer resolution: 5 kHz.

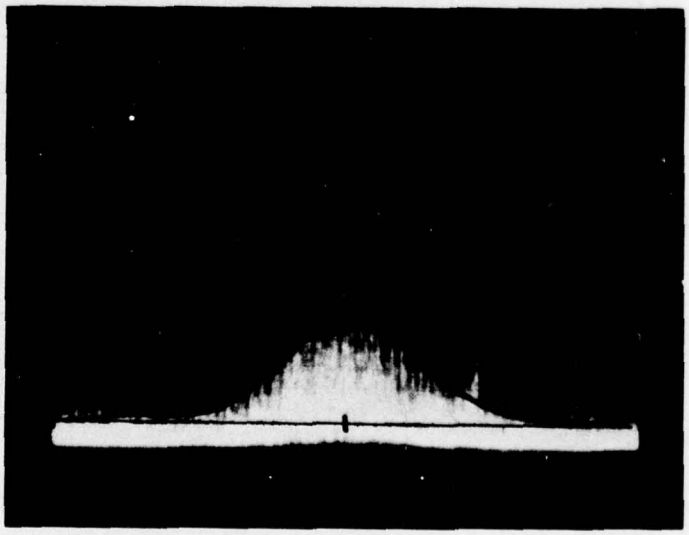

Fig. A.18. Microwave power spectrum near $\rho\delta$ = 8.19 GHz (100 kHz/div). Spectrum analyzer resolution: 5 kHz.

Now k is given by

$$k = k' + ik'' \simeq \frac{\omega}{c}\left[1 + \frac{\chi'(\omega)}{2}\right] + i\,\frac{\omega}{2c}\,\chi''(\omega) \tag{A.42}$$

where it has been assumed that the refractive index is unity and $\chi'(\omega)$ and $\chi''(\omega)$ are the real and imaginary parts of the susceptibility $\chi(\omega)$. $\chi'(\omega)$ and $\chi''(\omega)$ are not independent but are related through the Hilbert transform,[34]

$$\chi'(\omega) = -\frac{1}{\pi}\,PP\int_{-\infty}^{\infty}\frac{\chi''(\omega')}{\omega' - \omega}\,d\omega' \tag{A.43a}$$

$$\chi''(\omega) = \frac{1}{\pi}\,PP\int_{-\infty}^{\infty}\frac{\chi'(\omega')}{\omega' - \omega}\,d\omega' \tag{A.43b}$$

where PP stands for the principal value integral.

The laser mode frequency is then given by

$$f_n = \frac{nc}{2L}\left[1 + \frac{\chi'(\omega)}{2}\right]^{-1} \tag{A.44}$$

Consider now the frequency obtained by mixing the mth and $(m + \rho)$th modes (in the context of Chapter I).

---

[34] R. H. Pantell and H. E. Puthoff, *op. cit.*

$$f_\rho\Big|_{m,\ m+\rho} = f_{m+\rho} - f_m$$

$$= \frac{c}{2\ell}\left[(m+\rho)\left[1+\frac{\chi'\ f_{m+\rho}}{2}\right]^{-1} - m\left[1+\frac{\chi'\ f_m}{2}\right]^{-1}\right]$$

$$\simeq \rho\delta - \delta\left\{\frac{m+\rho}{2}\,\chi'\left(f_{m+\rho}\right) - \frac{m}{2}\,\chi'\left(f_m\right)\right\} \qquad \text{(A.45)}$$

where the assumption $\chi'(\omega) << 1$ was made. Now $\rho << m$ and $f_\rho\Big|_{m,\ m+\rho}$ can be written

$$f_\rho\Big|_{m,\ m+\rho} \simeq \rho\delta - \frac{\omega_o}{4\pi}\left[\chi'\left(\omega_{m+\rho}\right) - \chi'\left(\omega_m\right)\right] \qquad \text{(A.46)}$$

where ω_o is the center frequency of the laser line. The second term in Eq. A.46 represents the frequency shift in the mixed microwave frequency from $\rho\delta$. It is this term that needs to be considered.

For a gas laser operating far above threshold, $\chi''(\omega)$ will, to a good approximation, have a shape shown in Fig. A.19(a). What has been assumed in Fig. A.19(a) is that the laser far above threshold burns holes in the gain curve down to the lasing threshold level. These holes are so wide that they will depopulate the whole curve down to the threshold level, hence the "flat top" in Fig. A.19(a). Figure A.19(b) is the Hilbert transform of Fig. A.19(a). An analysis of $\chi'\left(\omega_{m+\rho}\right) - \chi'\left(\omega_m\right)$ shows the following results:

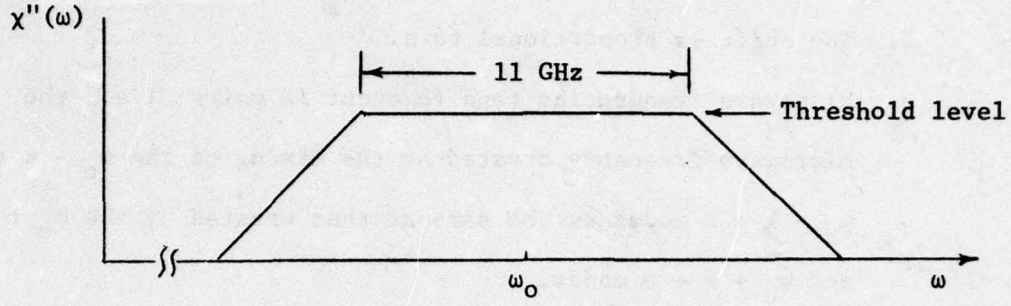

(a)

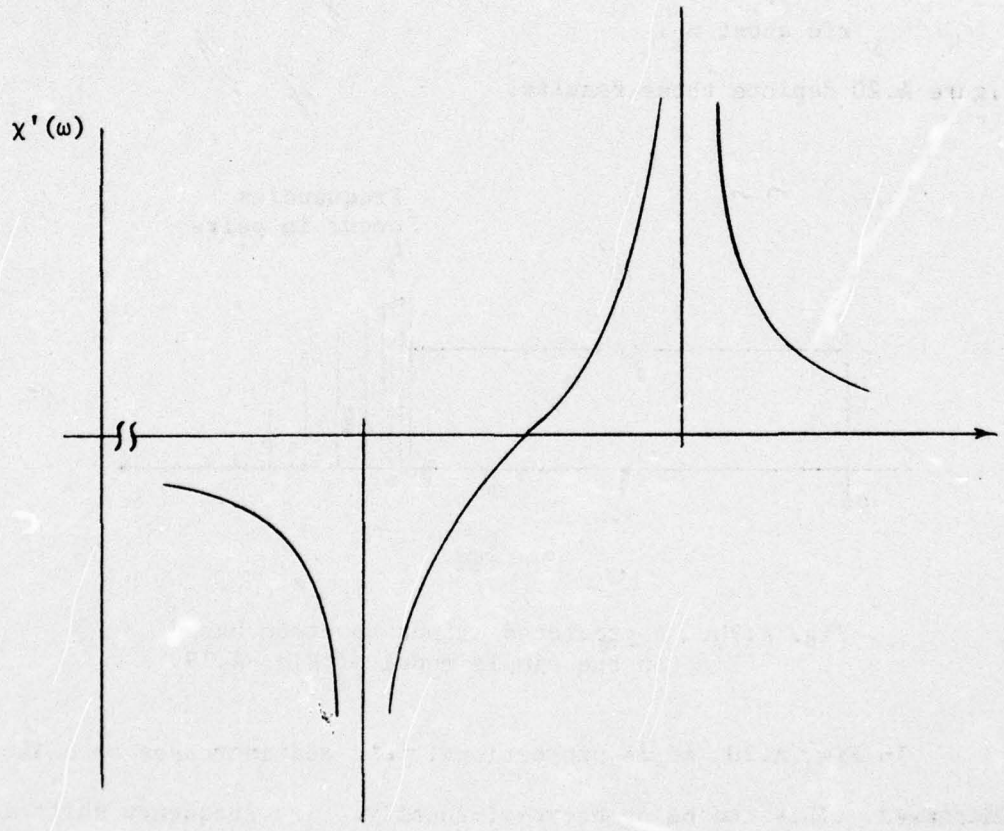

(b)

Fig. A.19. (a) An estimate of $\chi''(\omega)$ for a gas laser far above threshold; (b) the shape of $\chi'(\omega)$.

1. There is a positive shift in the microwave frequencies.
2. The shift is proportional to ρ.
3. Microwave frequencies tend to occur in pairs; i.e., the microwave frequency created by the mixing of the $m_o - k$ and $m_o - k + \rho$ modes is the same as that created by the $m_o + k$ and $m_o + k + \rho$ modes.
4. The "density" of the microwaves is not uniform.
5. The frequency shift is less for the mixing of modes symmetric about ω_o.

Figure A.20 depicts these results.

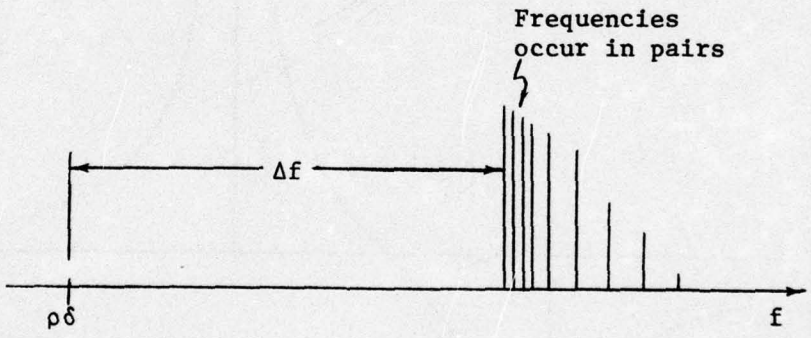

Fig. A.20. A predicted output spectrum based on the simple model of Fig. A.19.

In Fig. A.20, Δf is proportional to ρ and increases as ρ is increased. This can be seen experimentally. The frequency shift is really a function ratio of ρ to the width of the "flat top". The width of the "flat top" in Fig. A.19(a) depends on the threshold level. As the threshold is increased, fewer modes will oscillate and the

theory would predict that the microwave frequencies would shift farther from $\rho\delta$. This can be observed. The laser cavity contains a variable aperture; decreasing the aperture size increases the cavity loss and hence increases the threshold level. When this is done, the group of microwave frequencies near $\rho\delta$ displayed on the spectrum analyzer can be observed to increase in frequency a few MHz. As the aperture is opened, they decrease in frequency.

It is impossible to tell from the photographs anything about the pairing of microwave frequencies and little can be told about the density of frequencies. If anything, the density seems to be uniform. The predicted intensity versus frequency also seems to be lacking except in Fig. A.16 for $\rho\delta$ = 3.99 GHz. This could be due to three factors. First, the shape predicted in Fig. A.20 is highly dependent on the shape of $\chi''(\omega)$. If the top were not flat but were to have a wavelike dependence riding on top, the character of Fig. A.20 would be altered so that the maximum intensity is not on the extreme left. Second, there is a good possibility that mode competition effects could be responsible. The largest "predicted" intensities in Fig. A.20 are from those lines that would be most strongly coupled. Finally, the fact that the microwave frequencies tend to occur in pairs may have an effect. Consider again the output current of the diode as given by Eq. A.35:

$$|I_{\rho\delta}(\omega)|^2 = \left(\frac{e\eta}{hf}\right)^2 \sum_{\ell=-M/2}^{M/2-\rho} \delta\left(\omega - \omega_{\rho\ell}\right) \Bigg\{ P_\ell(t)P_{\ell+\rho}(t)$$

$$+ 2 \sum_{k>\ell}^{M/2-\rho} \sqrt{P_\ell(t)P_{\ell+\rho}(t)P_k(t)P_{k+\rho}(t)}$$

$$\cdot \cos\left(\phi_{\rho\ell} - \phi_{\rho k}\right) \cdot \delta\left(\omega_{\rho\ell} - \omega_{\rho k}\right) \Bigg\} \qquad \text{(A.47)}$$

The second delta function should not be taken too literally, what is really meant is a sharply peaked function near $\omega_{\rho\ell} - \omega_{\rho k} = 0$. If the frequency does occur in something like pairs (which the simple theory seems to predict), then near some $\omega' \simeq \omega_{\rho\ell}$ and $\omega_{\rho k}$,

$$\frac{|I_{\rho\delta}(\omega')|^2}{\left(\frac{e\eta}{hf}\right)^2} = P_\ell(t)P_{\ell+\rho}(t) + P_k(t)P_{k+\rho}(t)$$

$$+ 2 \cos\left(\phi_{\rho\ell} - \phi_{\rho k}\right) \sqrt{P_\ell(t)P_{\ell+\rho}(t)P_k(t)P_{k+\rho}(t)} \qquad \text{(A.48)}$$

Clearly now, $|I_{\rho\delta}(\omega')|^2$ depends strongly on the phase $\phi_{\rho\ell} - \phi_{\rho k}$, which is beyond any hope of being predicted. It should be noted at this point that the pairing of the frequencies is due solely to the symmetry of $\chi''(\omega)$. As long as symmetry is maintained, the frequencies should occur in pairs.

The exact explanation for the difference in shape of the predicted

and actual outlines of the frequencies is most likely a combination of all three causes. Also it should be remembered that the model is far from exact since different standing wave modes "burn holes" at different z-positions so that only a model that took this fact into account would have a chance of being accurate.

It is clear now that the meaning of height of the peak display on the spectrum analyzer is in some doubt. If the resolution of the spectrum analyzer is kept narrow enough, and remembering that the powers of the mixed frequencies should occur in pairs, then at any ω',

$$|I_{\rho\delta}(\omega')|^2 \propto P_{\ell}(t)P_{\ell+\rho}(t) + 2\sqrt{P_{\ell}(t)P_{\ell+\rho}(t)P_{k}(t)P_{k+\ell}(t)}$$

$$\cdot \cos\left(\phi_{\rho\ell} - \phi_{\rho k}\right) + P_{k}(t)P_{k+\rho}(t) \qquad \text{(A.49)}$$

Remember now that $\phi_{\rho\ell}$ and $\phi_{\rho k}$ will be functions of time. Consider a suitable time average of $|I_{\rho\delta}(\omega')|^2$. Define

$$\overline{P_{\ell}(t)P_{\ell+\rho}(t)} = \overline{P_{\ell}(t)}\ \overline{P_{\ell+\rho}(t)} + \varepsilon_{\ell,\ \ell+\rho}$$

where $\varepsilon_{\ell,\ \ell+\rho}$ is defined as the error in assuming $P_{\ell}(t)$ and $P_{\ell+\rho}(t)$ are independent variables. From the discussion of mode coupling, $\varepsilon_{-\rho/2,\ \rho/2}$ should be the largest error since these modes are most strongly coupled. As ℓ becomes different from $-\rho/2$, $\varepsilon_{\ell,\ \ell+\rho}$ should decrease rapidly. It is extremely difficult to estimate $\varepsilon_{\ell,\ \ell+\rho}$

since no strong signal theory for the case under consideration has been developed. If the modes at ℓ and $(\ell + \rho)$ and k and $(k + \rho)$ are not symmetric about ω_o, then the mode should decouple enough to permit the following statements:

$$\overline{P_\ell(t)P_{\ell+\rho}(t)} = \overline{P_\ell(t)}\ \overline{P_{\ell+\rho}(t)} \tag{A.50a}$$

$$\overline{P_k(t)P_{k+\rho}(t)} = \overline{P_k(t)}\ \overline{P_{k+\ell}(t)} \tag{A.50b}$$

If we also make the assumption that the ϕ's are independent of the P's and $\overline{\cos\ \phi_{\rho\ell} - \phi_{\rho k}} = 0$, then defining $P_\ell = \overline{P_\ell(t)}$, $|I_{\rho\delta}(\omega')|^2$ can be written

$$|I_{\rho\delta}(\omega')| = \left(\frac{ne}{hf}\right)\left(P_\ell P_{\ell+\rho} + P_k P_{k+\rho}\right) \tag{A.51}$$

Again, if $\chi''(\omega)$ is symmetric, $P_\ell P_{\ell+\rho} = P_k P_{k+\rho}$, hence

$$\Delta I_{\rho\delta}(\omega')| = 2\left(\frac{ne}{hf}\right) P_\ell P_{\ell+\rho} \tag{A.52}$$

Equation A.52 can be used to predict the peak average power expected from the diode. Using Eqs. A.18, A.38 (in using Eq. A.38 for $P_\ell P_{\ell+\rho}$, an upper limit is being found; this should not be too bad an approximation since $P_\ell P_{\ell+\rho}$ varies slowly with ℓ), and A.52,

$$\overline{P_{diode}(\rho\delta)}\Big|_{peak} = \frac{\left(\sqrt{2}\,\frac{\eta e}{hf}\right)^2 P_o^2\, e^{-\alpha\frac{\rho^2}{2}}}{i(2\pi)^2(\rho\delta)^2\, C_j^2 R_s^2\, |T_{22}(\rho\delta)|^2} \qquad (A.53)$$

Equation A.53 gives the upper limit on the peak average power out at any one instant. $P_{diode}(\rho\delta)\Big|_{peak}$ could be from zero to approximately twice the value given in Eq. A.53. Converting Eq. A.53 to dBm,

$$10\log_{10}\left[\overline{P_{diode}(\rho\delta)}\Big|_{peak}\right] = 20\log_{10}\sqrt{2}\,\eta + 10\log_{10}\left[\left\{8(2\pi)^2(\rho\delta)^2\, C_j^2 R_s^2\, |T_{22}(\rho\delta)|^2\right\}^{-1}\right] + 10\log_{10}\left[\left(\frac{e}{hf}\right)^2 P_o^2\, e^{-\alpha\frac{\rho^2}{2}}\right] + 30 \qquad (A.54)$$

The first term in Eq. A.54 has been written to separate out the quantum efficiency. The second term is proportional to the attenuation introduced into the circuit due to the mismatch between R_s and Z_o and the parameters C_j, C_B, and L. The third is proportional to the power introduced into the circuit by the laser. Equation A.53 or A.54 is the predicted average peak power expected from the photodiode as seen by a microwave spectrum analyzer. It corresponds to the average height of the peak of the power spectrum at any $\rho\delta$ (see Figs. A.15 through A.18).

In light of this discussion of Eq. A.35, consider Eq. A.31.

Again, if mixed frequencies occur in pairs, then terms containing $\cos\left(\phi_{\rho\ell} - \phi_{\rho k}\right)$ will occur, making the output dependent on the phases $\left(\phi_{\rho\ell} - \phi_{\rho k}\right)$'s. This will be the main problem in using Eq. A.31. If a suitable time average of Eq. A.31 is taken, then

$$\overline{i^2_{\rho\delta}(t)} = 2\left(\frac{\eta e}{hf}\right)^2 \sum_{\ell=-M/2}^{M/2} P_\ell P_{\ell+\rho} + 2\left(\frac{\eta e}{hf}\right)^2 \varepsilon_{\rho\delta} \qquad \text{(A.55)}$$

where the error $\varepsilon_{\rho\delta}$ is given by

$$\varepsilon_{\rho\delta} = \varepsilon_{-\rho/2,\ \rho/2} + \sum_{\ell=-M/2}^{M/2-\rho} \sum_{k>\ell}^{M/2-\rho} \sqrt{P_\ell P_{\ell+\rho} P_k P_{k+\rho}}$$

$$\cdot\ \overline{\cos\left[\left(\omega_{\rho\ell} - \omega_{\rho k}\right)t + \phi_{\rho\ell} - \phi_{\rho k}\right]}$$

(It has been assumed $\varepsilon_{\ell,\ \ell+\rho} =, \ \ell \neq -\rho/2$.) The size of $\varepsilon_{\rho\delta}$ will be difficult to estimate and will depend on the bandwidth of the "filter" used to take the time average so that where $\omega_{\rho\ell} \approx \omega_{\rho k}$, $\varepsilon_{\rho\delta}$ will be dependent of the phases $\left(\phi_{\rho\ell} - \phi_{\rho k}\right)$. Since a microwave spectrum analyzer was available for measuring the output power and a tunable band pass filter was not, no further consideration of Eq. A.31 will be given. It seems, however, that the complexity of using Eq. A.53 or Eq. A.54 is less than that of using Eq. A.55.

APPENDIX IX

EXPERIMENTAL PROCEDURE

A microwave spectrum analyzer was used to detect the diode output. Figure A.21 shows the basic experimental arrangement. A Spectra Physics model 166-03 argon ion laser was tuned to the 5145 Å line and operated at just under maximum power insuring a large number of oscillating longitudinal modes. An optical attenuator was constructed from an argon laser mirror and two neutral density filters to reduce the optical power from 2.3 watts to 89 mW. The attenuated optical power was measured with a Spectra Physics 401C power meter. The laser illuminated the diode surface. For measurement purposes, the diode and taper were considered to be one unit. An X-band and an S-band biasing-T were used to apply a reverse dc bias to the diode. S-band measurements were made directly at the RF output of the biasing-T. X-band measurements were made by first amplifying the signal using a Watkins-Johnson (WJ-3041) low noise TWT amplifier (7-11 GHz). A Tektronix 491 spectrum analyzer was used as a frequency sensitive power meter.

The system was calibrated using an X-band (HP-620A) and an S-band (HP-616A) signal generator and an HP-432A power meter with an HP-487A thermistor mount. The overall gain of the S-band biasing-T and X-band biasing-T in series with the TWT amplifier was found by observing the insertion loss (gain) at various frequencies using the spectrum analyzer as a detector.

Absolute power measurements were made using the RF signal

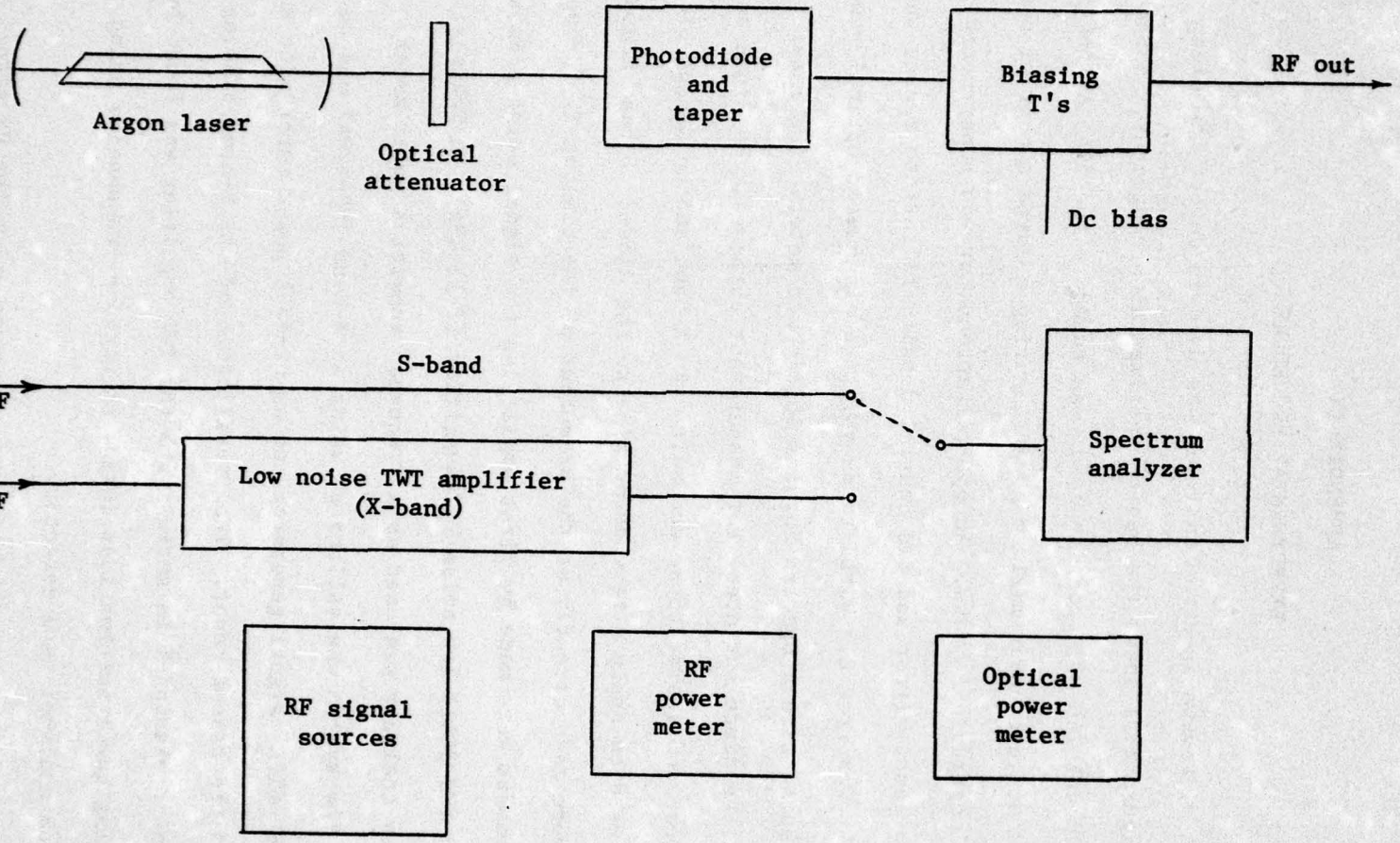

Fig. A.21. Basic experimental setup.

generator with the RF power meter to calibrate the spectrum analyzer at each measured frequency.

Measurements were made at several frequencies in both S- and X-bands. At every measured frequency, the spectrum analyzer was calibrated against the known source generator. The reading taken was the average peak value on the output spectrum. Power readings could be taken up to about 9.5 GHz; however, past this point, the signal-to-noise ratio was too small to make meaningful measurements. However, signals could be detected up to about 10.5 GHz. Each of the measurements was corrected to take into account the gain of the biasing-T's and TWT amplifier (X-band only). The results of these measurements are shown in Fig. A.22. The possible error in estimating the average peak output was ±2 dB.

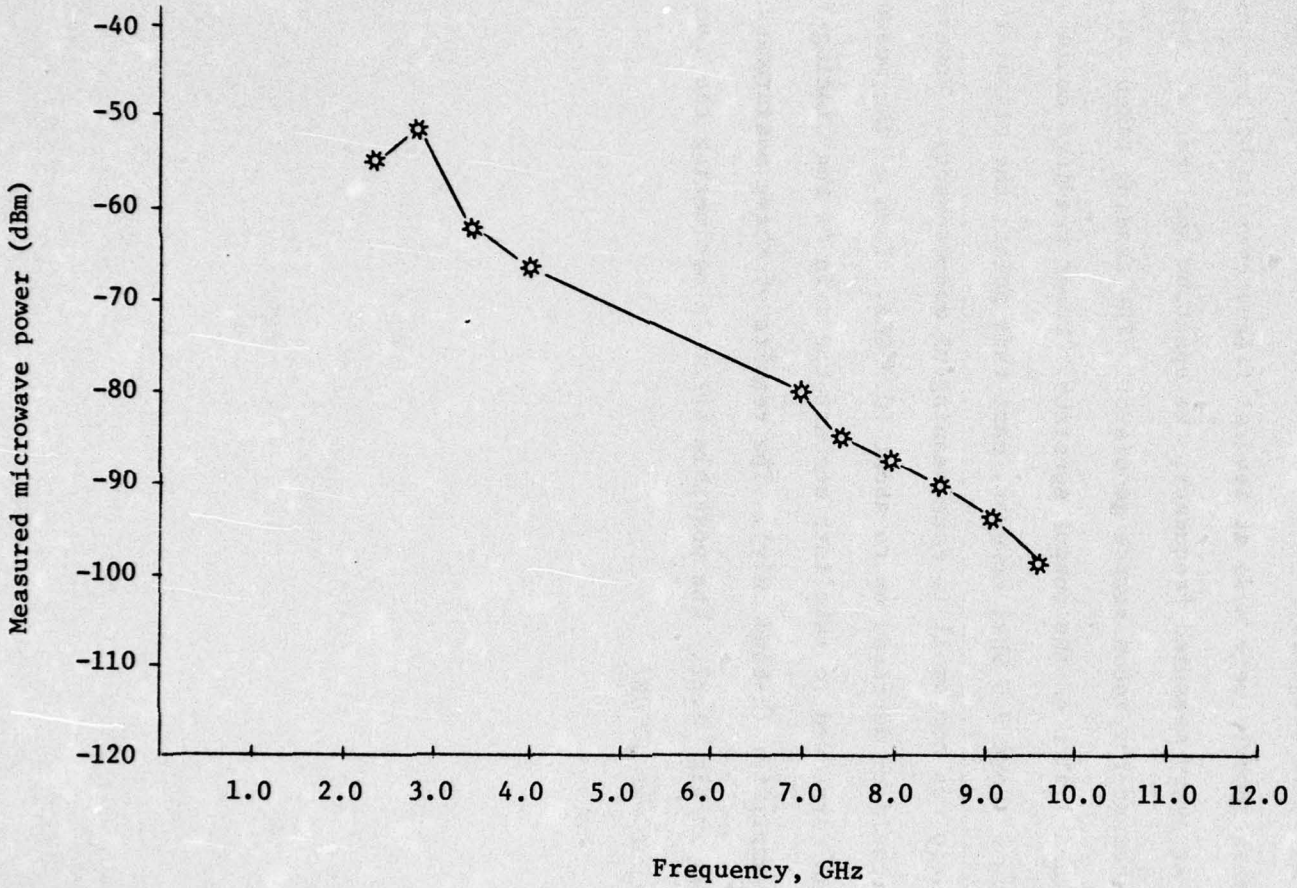

Fig. A.22. Measured microwave power output (P_L = 6 mW).

APPENDIX X

PREDICTED RESPONSE

Equation A.54 was used to plot a predicted response curve. There is still a small problem to be rectified. It has been assumed that the power in the nth mode (n = 0, ±1, ..., ±M/2) is given by

$$P_n = P_o\, e^{-\alpha n^2} \tag{A.56}$$

This is not quite true. For some n, say m, $P_m = 0$, since the laser has a threshold, and the gain at ω_m will not be great enough to overcome the losses. To rectify this problem, instead of using Eq. A.56 for P_n, the following approximation was used in the calculations to rectify the problem of the threshold power:

$$P_n = P_o \left(e^{-\alpha n^2} - e^{-\alpha m'^2} \right) \tag{A.57}$$

and in Eq. A.54,

$$P_o\, e^{-\alpha \frac{\rho^2}{4}} \rightarrow P_o \left(e^{-\alpha \frac{\rho^2}{4}} - e^{-\alpha \frac{m'^2}{4}} \right) \tag{A.58}$$

This change does not affect any of the previous conclusions. m' will be greater than M/2.

A program was written which accepts values for the circuit

parameters R_s, Z_o, R_{sh}, C_j, C_B, and L along with values for α, m', M, and the total laser power incident on the photodiode surface, P_2. The parameter P_o is calculated according to

$$P_o = \frac{P_L}{1 + 2 \sum_{n=1}^{M/2} \left(e^{-\alpha n^2} - e^{-\alpha m'^2} \right)} \tag{A.59}$$

Measurements from the photos of the laser power show $\alpha \simeq 0.0011$. The incident laser power, P_2, was calculated using the total laser power, the known surface area of the diode, and the gaussian beam parameters. P_L was found to be 6 mW. Detecting microwave power at ≃10.5 GHz indicates at least 92 modes were lasing. For the calculations, it was assumed that two more modes were lasing on either side of the gain curve whose mixed frequencies could not be detected, so that a total of M = 96 modes was assumed in the calculations. Values of m' = (M + 1)/2 to ∞ were used.

The output of the program was a plot versus frequency of the predicted microwave power, $P_{\rho/2}$ (the laser power), and the second term in Eq. A.59 describes the circuit. Figure A.23 shows the predicted output for $\sqrt{2}\,\eta = 1$, $R_s = 1\ \Omega$, $Z_o = 2\ \Omega$, $R_{sh} = 10^8\ \Omega$, $C_j = 4$ pF, $C_B = 0.02$ pF, and L = 0.75 nH for the cases m' = 1 and m' = ∞. In general, there is a resonance at $\omega^2 = 1/LC_j$. For Z_o large enough, the resonance cannot be seen. The effect of the parameter m' can be seen in Fig. A.23. The case of m' = ∞ corresponds to using Eq. A.56. The

AD-A034 173 UTAH UNIV SALT LAKE CITY MICROWAVE DEVICE AND PHYSI--ETC F/G 17/8
SOLID STATE OPTICAL DETECTOR.(U)
AUG 76 R W GROW, J R BOYE, C K PETERSON N00014-67-A-0325-0005
UNCLASSIFIED UTEC-MD-76-233 NL

2 OF 2
AD
A034173

END
DATE
FILMED
2-77

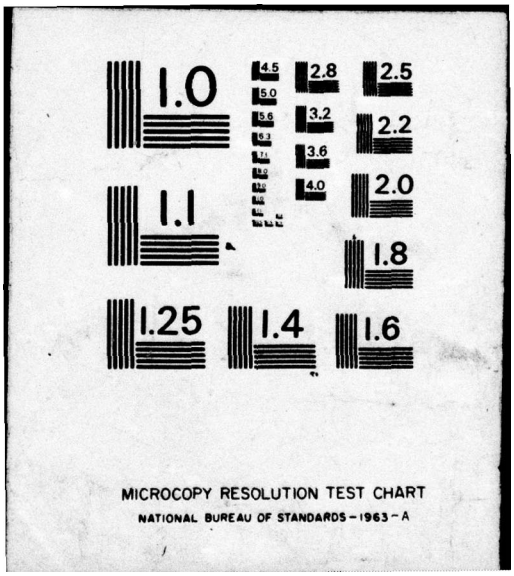
1.0
1.1
1.25
1.4
1.6
1.8
2.0
2.2
2.5
2.8
3.2
3.6
4.0
4.5
5.0
5.6
MICROCOPY RESOLUTION TEST CHART
NATIONAL BUREAU OF STANDARDS - 1963 - A

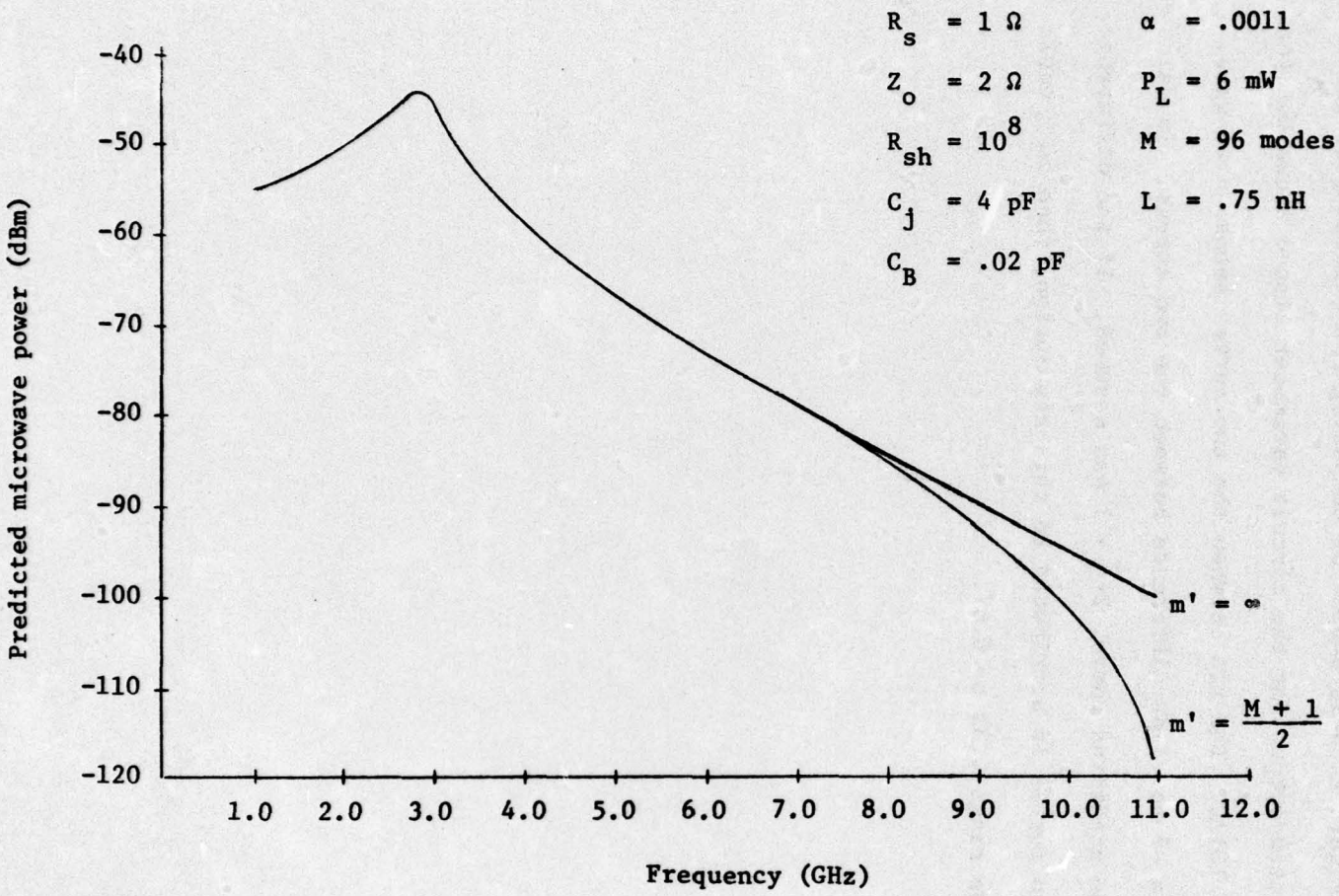

Fig. A.23. Predicted microwave power.

cases $m' = 1$ and $m' = \infty$ set the boundaries on the region of possible output. Figure A.24 is a plot of comparing the experimental curve to the predicted output for the circuit parameter listed above but for $m' = (M + 10)/2$. The fit between the two curves seems quite good. There is a -7 to -1 dB difference between the two curves. In calculating the predicted curve, $2\sqrt{\eta} = 1$ was assumed. If the difference in the two curves is attributed to this assumption, then an η would lie in the range 0.32 to 0.67.

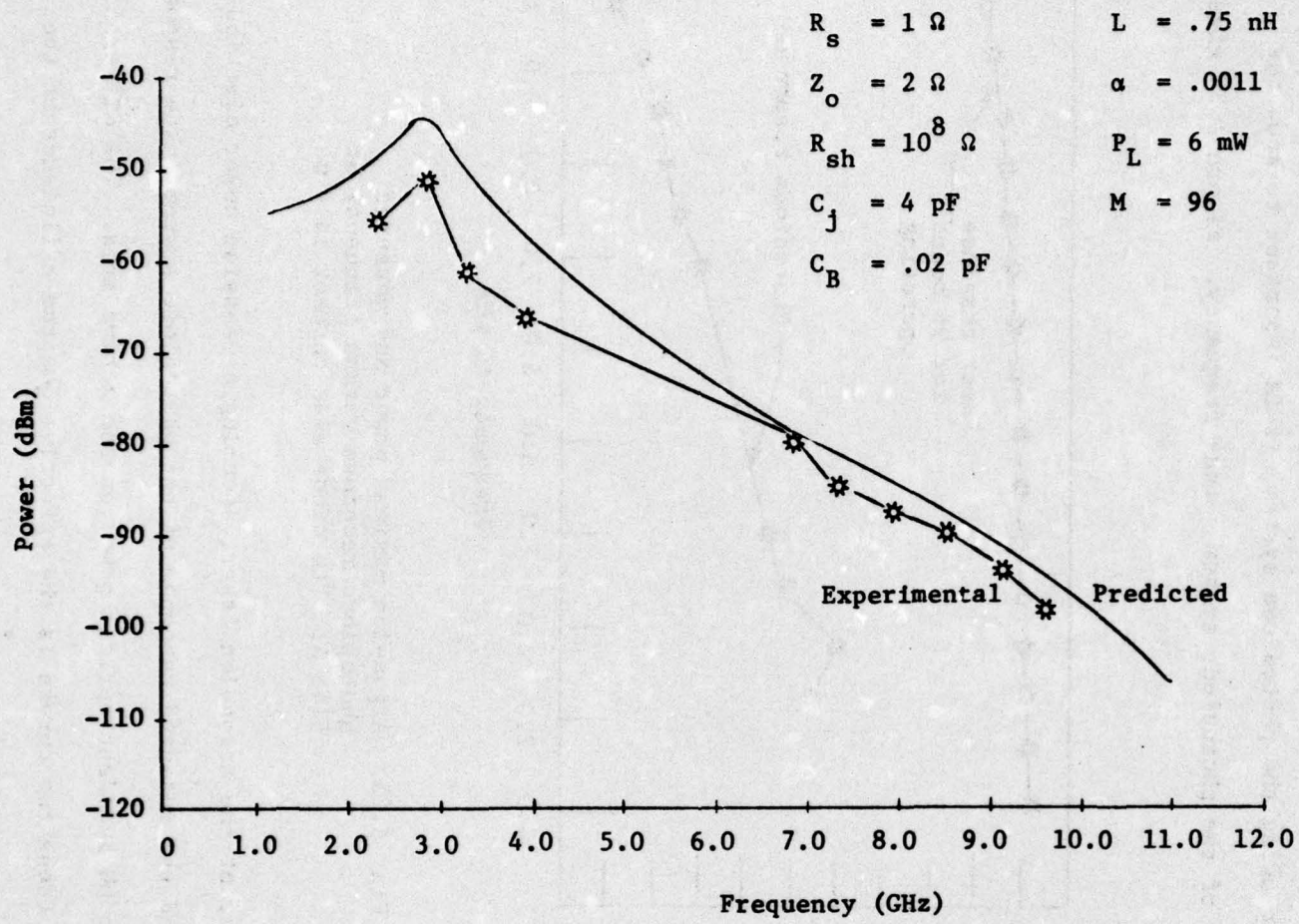

Fig. A.24. Comparison of predicted and experimental microwave power curves.

APPENDIX XI

EFFECTIVE QUANTUM EFFICIENCY

In using the photodiode system, it is important to know the response of the photodiode system versus frequency. Figure A.25 gives

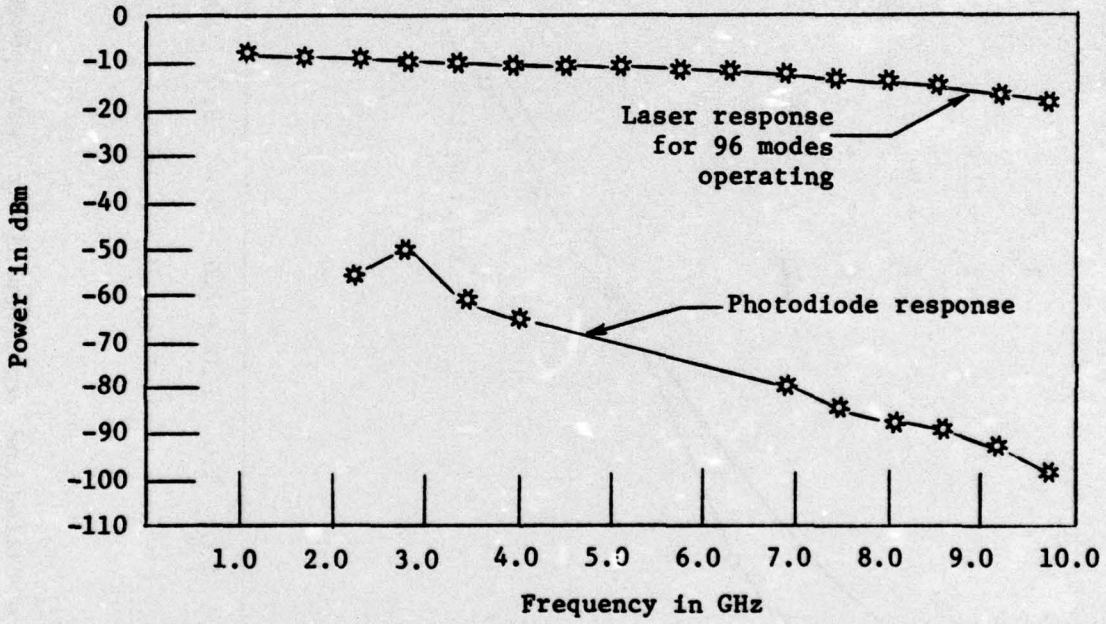

Fig. A.25. Argon-ion maximum power and measured photodiode response versus frequency at 5145 Å. The diode bias current is 4 mA.

the power of the argon-ion laser, assuming a Gaussian power distribution, and the measured response of the photodiode system. The response is for 6 mW incident optical power on the active area. The difference between these two curves is the effective quantum efficiency of the photodiode system at 5145 Å. This is shown in Fig. A.26.

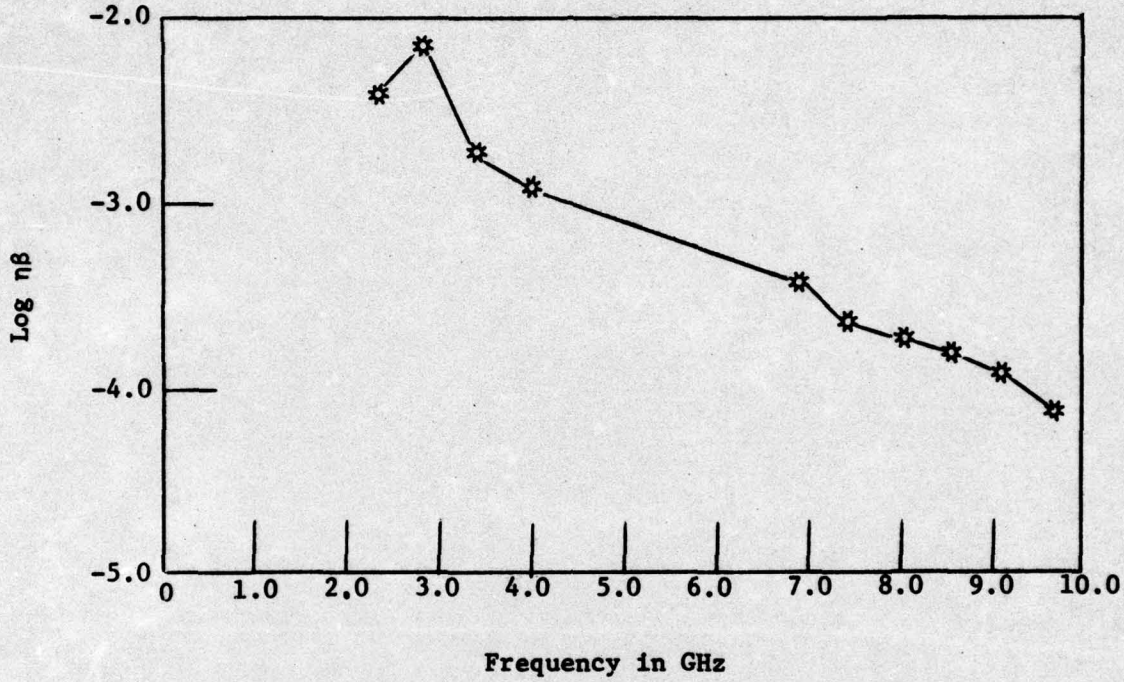

Fig. A.26. Effective quantum efficiency of photodiode system versus frequency.